

A GPS-Reflections Receiver That Computes Doppler/Delay Maps in Real Time

Oleguer Nogués-Correig, Estel Cardellach Galí, Josep Sanz Campderrós, and Antonio Rius

Abstract—This paper describes a new instrument that was specially designed and developed to gather global positioning system (GPS) signals after they have been reflected from suitable surfaces (sea, ice, and ground), for Earth remote sensing. The device has been called the GPS open-loop differential real-time receiver (GOLD-RTR). Its main and most innovative feature is its computation and storage, in real time, of complex-valued (I and Q) cross correlations (waveforms) between GPS L1-C/A signals—received directly and after reflection—and the corresponding models of these signals. Particularly, the GOLD-RTR schedules consecutive coherent integration time slots of 1 ms over which ten parallel correlation channels, with 64 lags each, work simultaneously and continuously with the input raw data sampled at 40 MHz. The total throughput is 10 000 waveforms per second, each waveform being 64 lags long. These real-time correlation resources can be flexibly distributed in several configurations according to the observational requirements, for instance: Doppler/delay maps or up to ten simultaneous reflected waveforms for ten different GPS satellites are examples of what can be done. The further processing of the real-time computed 1-ms waveforms in a flight campaign over the ocean, ice, or ground can be used to obtain geophysical parameters such as sea level and tides, sea surface mean-square slopes, ice roughness and thickness, soil moisture and biomass, or future applications. This paper covers the GOLD-RTR architecture and hardware, signal processing and data storage issues, machine–user interface, laboratory readiness tests, and waveform data samples from the first two jet aircraft campaigns at 9300 m over the sea.

Index Terms—Altimeter, bistatic radar, global positioning system reflections (GPS-R), GPS open-loop differential real-time receiver (GOLD-RTR), passive reflectometry and interferometry system (PARIS) concept, radar systems, real-time correlation, scatterometer, waveforms.

I. INTRODUCTION

THE WORKING principle of radar systems is the observation of electromagnetic radiation, scattered from distant objects that have been illuminated by a radiating source in order to remotely study certain physical properties of the object. Ever since the first monostatic radars appeared, the scattering process of electromagnetic energy from objects has been extensively studied, with applications in the field of Earth remote sensing and in the exploration of other planets and moons of the solar system [1]. The global positioning system

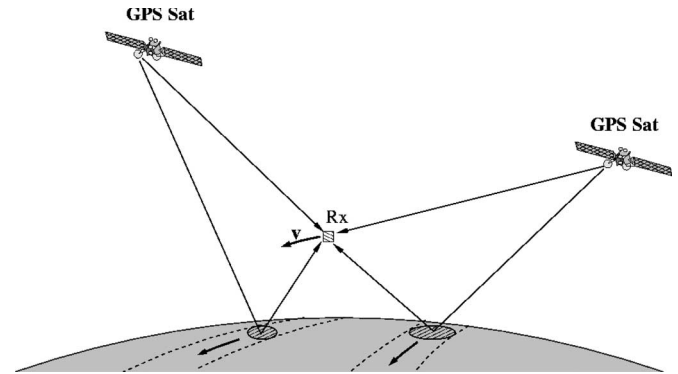


Fig. 1. Passive reflectometry and interferometry system (PARIS) scenario sketch [2]. A vehicle flying at a certain speed over the ocean observes the navigation signals emitted by GPS satellites, both direct rays and forward-scattered rays after they are reflected on the sea surface. The difference in time of arrival (TOA) between direct and reflected signals provides information about altimetry, whereas the shape of the reflected signal provides information about sea surface characteristics.

(GPS) open-loop differential real-time receiver (GOLD-RTR) instrument described in this paper has been developed to observe the navigation signals emitted by GPS satellites, both direct rays propagated through the line of sight (LOS) and reflected forward-scattered rays from the Earth's surface (bistatic geometry). This configuration was first proposed in 1993 by the European Space Agency (ESA) as a passive multistatic radar to monitor mesoscale ocean altimetry [2]. Such a scenario is depicted in Fig. 1. From then on, in-depth work has been performed to study the strong points and applications of GPS-reflections (GPS-R). The focus of this work has been in: 1) altimetry experiments using models of the envelope of the reflected signals, either from a static position [3] or from aircraft altitudes [4]–[7]; 2) altimetry experiments that mainly use information from the less noisy phase of the reflected signal instead of the envelope, both from static positions near the reflective surface [8]–[13] or from a Low Earth Orbiter (LEO) altitude using data from the Challenging Minisatellite Payload for Geophysical Research and Application (CHAMP) GPS radio occultations satellite [14]; 3) scatterometry experiments to retrieve ocean surface states [15] such as wind [16]–[18] or sea roughness [19]; 4) basic theoretical models that describe the dependence of sea roughness on wind [20], scatterometric models that describe the dependence of the GPS-reflected signal shape on wind [21]–[24], and theoretical studies of the polarization properties of the GPS-reflected signals [25]; 5) applications for the characterization of soil moisture [26] and sea ice [27]; and finally, 6) space observations of GPS-R, first analyzing a few seconds of the Spaceborn Imaging Radar version C (SIR-C)

Manuscript received March 2, 2006; revised July 14, 2006. The campaigns were funded in part by the Spanish National Space Plan (ESP2004-00671, ESP2005-03310).

O. Nogués-Correig, E. Cardellach Galí, and A. Rius are with the Institut de Ciències de l'Espai, Institut d'Estudis Espacials de Catalunya (CSIC-IEEC), 08193 Barcelona, Spain (e-mail: nogues@ieec.fcr.es).

J. Sanz Campderrós was with the Institut de Ciències de l'Espai, Institut d'Estudis Espacials de Catalunya (CSIC-IEEC), 08193 Barcelona, Spain. He is now with ENFASYSYSTEM S.L., 08030 Barcelona, Spain.

Digital Object Identifier 10.1109/TGRS.2006.882257

calibration data [28], later using GPS radio occultation data from the CHAMP mission [14], [29] and even a dedicated GPS-R instrument aboard the U.K. Disaster Monitoring Constellation (UKDMC) satellite [30], providing the best opportunity thus far to observe GPS-R from space. This brief summary clearly shows that the emphasis has been put on the basic scientific demonstration of the possibilities of GPS-R. Specific instrumental developments, necessary to obtain more and better quality data, have received less attention. The GOLD-RTR aims to fill this gap and substantially improve GPS-R instrumentation. In order to highlight the differences and improvements between GOLD-RTR and previous instrumentation, a review of the latter is provided. From now on, it will be assumed that the reader is familiar with the GPS system and the structure of its navigation signals. A good summarized review of GPS receivers and signal structure can be found in [31], or [32], which is more extensive. For a precise official information on GPS user interface specification, refer to [33] and [34].

II. PREVIOUS INSTRUMENTATION

Previous GPS-R instrumentation can be divided into two groups: *software receivers* and *hardware receivers*. The architecture of software receivers is built around a set of multiple radio-frequency (RF) front-ends, which are all supplied by the same local oscillator (LO) for coherent conversion to baseband (BB). After the analog-to-digital (A/D) conversion and sampling, all the raw signal samples are directly dumped in a mass-storage medium without any kind of cross-correlation processing. This processing takes place offline in the laboratory, after the experiment, using dedicated software routines. The processing consists of cross-correlating the raw signals with local GPS ranging-signal replicas of the pseudorandom noise (PRN) codes, appropriately frequency shifted to account for the Doppler shift and LO residuals of the received signal. This is called the preprocess or correlation process and is performed using software on a standard computer with the experimental raw data retrieved from the files. The resulting products of this process are closely spaced samples of the cross-correlation function, evaluated over a few chips of PRN code around the correlation power peak, forming the so-called *waveforms*, which are actually the signals used for geophysical exploitation. The following are examples of software receivers:

- 1) *ESA instrumentation-A*, based on the GEC-Plessey GPS development kit [35] for conversion to BB and sampling (the same downconversion approach as in National Aeronautics and Space Administration (NASA) Langley Research Center instrumentation, see below) and a Signatec data acquisition (DAQ) card with 32 MB of run recording capacity. With this amount of memory, it was only possible to acquire continuous raw data in blocks of 2.56 s. After each acquisition, data were dumped from the DAQ to a digital tape. Each dump operation took about 10 min, thus enabling to record about 80 s of cumulative data after 4–5 h of continuous operation. An experiment using this setup is reported in [3].
- 2) *Jet Propulsion Laboratory (JPL) NASA instrumentation*, based on modified TurboRogue GPS receivers [36], [37] that provided the I and Q components of both the L1 and L2 GPS signals. The raw sampled data for both the direct and reflected signals was first synchronously and continuously recorded to a SONY SIR-1000 recorder [38], and later onto the hard disk, with virtually no limitation on data recording lengths. Specific software routines implementing a full GPS software receiver were also available during the postprocessing stage. A complete description of this instrument is found in [39], while [5] describes the experiments and results achieved in implementation.
- 3) *ESA instrumentation-B* was used on several experiments in [6], [7], and [10], based on modified TurboRogue GPS receivers and two SONY SIR-1000 recorders (similar to JPL's). This setup recorded only the I component of the BB signal. Moreover, certain sophisticated procedures were necessary in order to time-align the direct and reflected raw signals, which were dumped to two separate manually operated recorders.
- 4) *Versatile GPS receiver* developed by the Johns Hopkins University Applied Physics Laboratory. The system front-end is a GEC-Plessey chip [35], and direct and reflected data were synchronously sampled at 5.714 MHz by a high-speed recording system. Upon postprocessing, a software-based GPS receiver (with delay and Doppler tracking capabilities) was applied to both direct and reflected signals to obtain the waveforms. A description of this software receiver can be found in [40], while [24] and [41] describe an analysis of experimental data collected by this system.
- 5) *Catalan Institute for Space Studies (IEEC) instrumentation*, which was designed and built from scratch by the Polytechnic University of Catalunya (UPC, Barcelona, Spain). Its features are similar to JPL NASA Instrumentation, only differing in that it is integrated and assembled in a small and portable 12-kg rack and that it does not have L2 frequency signals. Specific software GPS receiver routines were written for processing the L1, C/A codes. A description of the system's hardware is found in [42], while [12] reports on experimental data and results achieved with it. The instrument data recording hardware is covered by a Spanish patent [43].
- 6) *University of Colorado (at Boulder) instrumentation*, based on two small GPS antennas mounted at the top and bottom of an aircraft to gather direct and reflected signals. Signals are down-converted to BB, raw sampled, and stored to hard disk drives for postprocessing. A reference to this system can be found in [44].
- 7) *Starlab Oceanpal instrumentation* based on two antennas mounted above and below a circular metallic ground plane, which is sustained near the coast, in order to separately pick up the direct and reflected signals over the ocean. The system has two analog downconversion chains and a raw data sampler system at 16 MHz. Record lengths of raw data are performed and stored on a data management unit. On completing a record, this unit automatically computes the complex waveforms and analyzes it further to derive geophysical products. The system is

connected to the web, so the results are available online. A description of this system can be found in [45].

- 8) *Surrey Satellite Space Center (SSTL) instrumentation*, which was flown in the UKDMC LEO satellite as an opportunity instrument for gathering GPS-R from space. The instrument is based on a GEC Plessey GPS chip set [35], and the raw sampled data are stored in a mass memory to later be downloaded to Earth for postprocessing. A description of this instrument, as well as some preliminary results, can be found in [30].
- 9) *NAVSYS Corporation* has developed several instruments based on one or more digital front-ends (DFEs) and a high-speed recording system. One of the latest developments consists of an antenna array of 109 elements [46]. The RF output of each antenna array is digitized by DFE and stored to a high-speed recording system. Upon postprocessing, a digital antenna beam steering and correlation process is performed using software. This system is capable of simultaneous multibeam steering, with the advantage of having a greater antenna gain.

There are clearly major differences in performance, capacity, and scope between the reviewed software receivers. However, the main limitation is still the fact that: they all require an intensive cross-correlation postprocess which involves the use of software routines, a good knowledge of how to operate them properly with the raw recorded data, and a considerable amount of time to run these routines and obtain results (at least when running on a standard computer). This is not a comfortable framework for the scientific end user, whose main interest is the analysis of the observable data: the waveforms obtained after postprocessing. With regard to this issue, a better GPS-R instrument would perform the cross-correlation postprocess in real time during the execution of the experiment, so that after experimentation the desired waveforms would be available as they would have been automatically computed without any human intervention. This instrument is called *hardware receiver*, featuring special digital hardware that computes the waveforms in real time. Until now—as far as the authors are aware—there are two precedents of such types of GPS-R receiver.

- 1) *NASA Langley Research Center instrumentation* measures the power of the signal reflected off the sea surface, as a function of the reception time. A geometric model giving the reflected signal's reception time relative to the direct signal is used to temporally position 12 single-lag correlators with $\sim 0.5 \mu\text{s}$ (150 m) spacing. The system provides waveforms obtained by coherent integration over 1 ms, which are then incoherently integrated over 0.1 s. Its features are: 5.7-MHz sampling rate, 12 single-lag correlators for waveform sampling, and the technology used is a commercial off-the-shelf (COTS) 2021 GEC Plessey [35] correlator chip. This makes the construction of a multicorrelator receiver difficult and expensive, and leaves very little room for flexibility in terms of custom digital hardware improvements. A description of this receiver is found in [17] or [21]. This type of instrument has been used by several groups in the U.S., e.g.,

Goddard Space Flight Center, University of Colorado, and also in Spain at IEEC [18].

- 2) *GFZ instrumentation*, based on the OpenGPS receiver hardware and software [47], measures the amplitude and phase of two lags of the direct signal arm (which is tracked), as well as the amplitude and phase of two lags of the reflected signal arm (which is obtained using a geometric open-loop model relative to the direct). The lags obtained by correlation are sampled at 50 Hz. This is done simultaneously for a maximum of four satellites. The lag separation for both the direct or reflected arms is $\sim 0.5 \mu\text{s}$ (150 m). Since the hardware is also based on the GEC Plessey GPS chipset [35], this instrument has the same limitations as that of the NASA Langley Research Center. Experiments performed with this setup were used to retrieve the ocean height [48].

In order to overcome the difficulties found in previous instrumentation, the GOLD-RTR instrument was designed to accomplish two main goals: 1) the instrument performs all the cross-correlation (waveform) computations automatically and in real time, during the execution of the experiment, and without any need for human intervention; and 2) the instrument has a set of 640 single-lag *I* and *Q* correlators, grouped into ten 64-lag independent correlation channels that work simultaneously, so that each channel can be loaded with its own signal model independent of the others. The lag spacing is ~ 50 ns (15 m). There is flexibility in the loaded signal models in order to force offset-values in delay or frequency, for both direct and reflected signals. All these features make it possible to assign different satellites to different channels or to assign the same satellite to all channels, but with slight differences in the delay model so as to produce a fine-delay map, or even to assign the same satellite to all the channels, but with slight differences in the frequency model so as to produce a Doppler/delay map or Doppler/delay map of two polarizations of a satellite signal, or other possible combinations.

III. INSTRUMENT HARDWARE

The instrument has been split into two physical devices: a 19-in rack that contains the front- and back-end electronics, and a laptop which provides control and monitoring functions of the rack electronics as well as disk storage for the recorded waveforms. Both parts communicate through a full-duplex Ethernet link at 100 Mbits/s, using a standard unshielded twisted pair (UTP) cable ended with RJ-45 connectors. This setup is shown in Fig. 2.

A. Interface

The rack interface is in the back panel, providing the following.

- 1) *Antenna inputs*. Three-jack N-type antenna input connectors are provided. Each one corresponds to the three downconversion channels inside the rack. Input RF impedance is 50Ω . This number of antenna inputs enables the use of an up-looking (direct links, navigation) and two



Fig. 2. View of the GOLD-RTR instrument setup. Below are the rack electronics and the back panel interface. The three-jack, N-type antenna input connectors, the power connector and switch, the ventilation outlets, and the Ethernet connector can be identified. The UTP cable links the rack and the laptop; the latter stores the real-time computed waveforms sent through the Ethernet.

down-looking antennas (reflected links) for polarimetry, interferometry, etc.

- 2) *Ethernet connector*. A female RJ-45 Ethernet connector is the communications interface between the rack and laptop electronics.
- 3) *Power connector* providing three lines: active, neutral, and ground. This instrument operates at 220 V ac and 50 Hz. Rack power consumption is 50 W.
- 4) *Power switch* to power on and off the rack electronics; also, there is a small box with a 0.5-A security fuse.
- 5) *Cooling fan holes* ventilation outlets to provide the appropriate electronics air-cooling. Must be left unobstructed.

B. Block Diagram

A summarized block diagram of the rack electronics is shown in Fig. 3. There are two main blocks: the RF front-end and the signal-processing back-end. The former is composed of: 1) three I and Q direct downconversion chains (downconverters) with their corresponding three antenna inputs; 2) the LO synthesizer that feeds them coherently with a common-tone down-shifted 300 kHz from the L1 carrier; and 3) the system reference oscillator, operating at 40 MHz. The back-end is composed of: 1) a one-bit A/D conversion stage (six comparators performing sign extraction) that converts the three I and Q BB pairs to digital; 2) the real-time signal processor that computes the waveforms; and 3) a commercial GPS receiver card that computes the navigation solution from antenna input 1. Note the coherence between the LO synthesized tone, the GPS receiver clock, and the signal-processor clock. The system works as follows: antenna input 1 should always receive direct GPS signals from a zenith pointing antenna, so that the GPS navigation card can compute the navigation solution, extract observable data from all the GPS satellites in view, and steer the 40-MHz system clock frequency to the GPS time rate. These direct signals are also I and Q downconverted. Antenna inputs 2

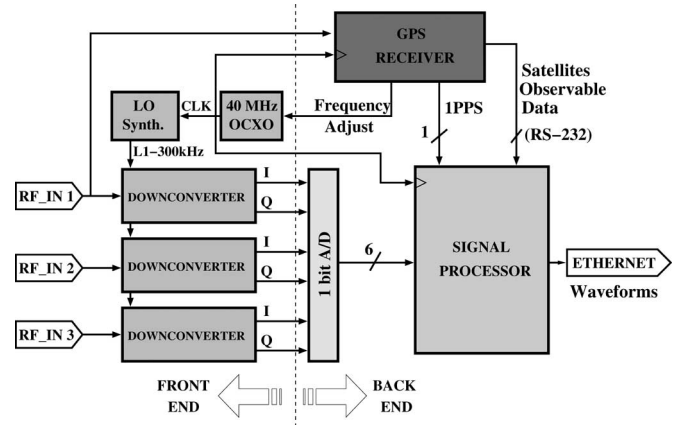


Fig. 3. Block diagram of the GOLD-RTR instrument rack electronics. The RF front-end performs direct downconversion of the GPS signals from RF to BB. The back-end provides enough signal-processing resources to track all the satellites in view (GPS receiver) and to compute in real time the desired waveforms for both direct and reflected signals (signal processor). The system has a unique reference 40-MHz timing signal, so that the downconversion beat tone and digital electronics clock reference are synchronous.

and 3 provide a means of connecting two separate nadir pointing antennas to gather the GPS-R for further downconversion to BB. The three I and Q BB pairs are synchronously one-bit A/D converted at a rate of 40 MHz and then passed to the signal processor. The signal processor, with the aid of the one-pulse-per-second (1PPS) timing signal and the satellite observable data, is able to continuously compute and precisely align signal models of the input signals, for the real-time production of 64-lag cross-correlation sequences (waveforms). The lag spacing in these sequences is ~ 50 ns. Since the signal model parameters are extracted from the satellite observable data provided by the external GPS receiver, parameter estimation is Open Loop: the signal processor does not have any acquisition or tracking capability that can extract the timing parameters (C/A code alignment and Doppler). That is why the instrument is called the GPS Open Loop Differential Real-Time Receiver. The term *differential* stands for the altimetric application. Complete details of signal-processing issues are given in Section IV.

C. Front-End

The front-end electronics are distributed on one shelf that fits in the 19-in rack, as shown in Fig. 4. The RF signals enter the system through the three antenna inputs and pass through a bias-tee (1), that provides a means of feeding external amplifiers through the coaxial antenna cable. External LNA effective amplification should be about 20 dB. The following stage consists of a 33-dB amplifier (2) that increases the signals' strength to the required levels in order to feed the input of the direct downconverters (7). Antenna input labeled 1 previously passes through a two-way power splitter (3), so that this signal is available to the GPS navigation card in the back-end (see Fig. 5). The GOLD-RTR 40-MHz reference oscillator (5) is steered to the GPS rate through the *Frequency adjust* signal coming from the aforementioned GPS receiver. The 40-MHz signal clock is outputted through the *Clock out* line to make

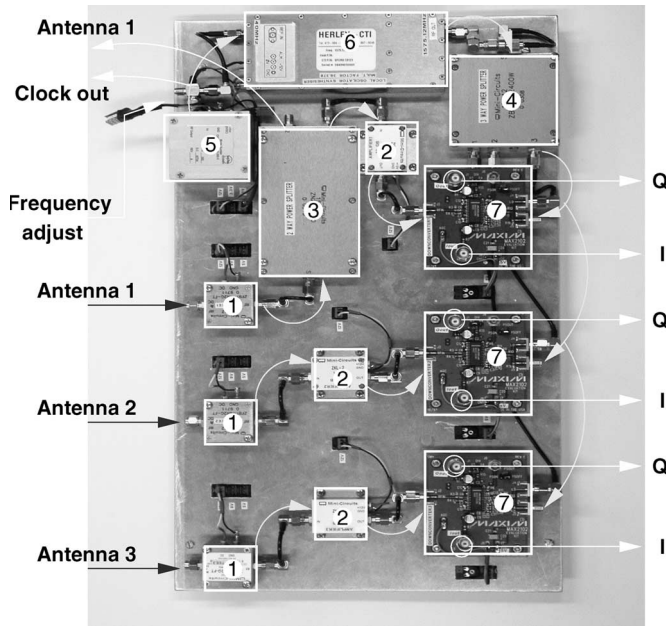


Fig. 4. Front-end shelf top view. Different subsystems are labeled with numbers. (1) Minicircuits ZFBT-4R2G-FT bias tee. (2) Minicircuits ZKL-2 33-dB amplifier. (3) Minicircuits ZN2PD2-50 two-way power splitter. (4) Minicircuits ZB3PD-2400W three-way power splitter. (5) Tech-time OV11-40-15-1-40.000-5 ovenized 40-MHz XO. (6) Herley-CTI PCRO LO synthesizer. (7) Maxim MAX2102 direct downconversion tuner-IC evaluation kit.

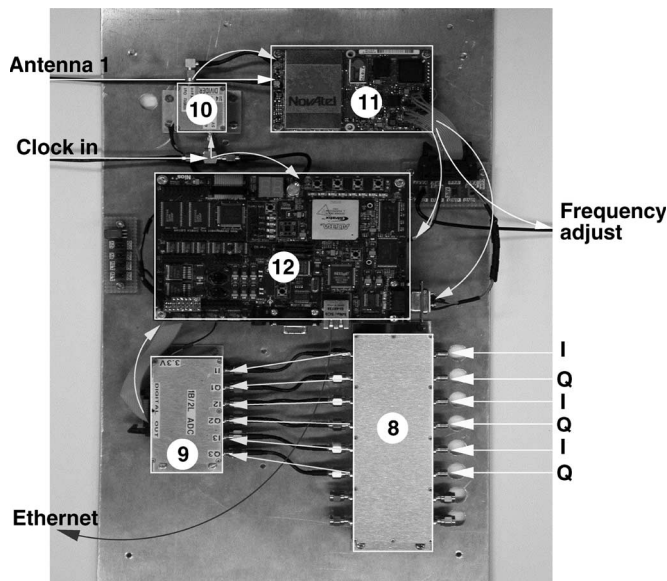


Fig. 5. Back-end shelf top view. Different subsystems are labeled with numbers. (8) Custom array of minicircuits SCLF-8 LPFs. (9) Custom array of Maxim MAX961 fast comparators to perform the one-bit A/D. (10) Custom frequency divider based on a Texas Instruments CD74ACT163 synchronous four-bit counter and a minicircuits SCLF-8 LPF. (11) Novatel OEM4-G2L L1/L2 GPS receiver [49], [50]. (12) Altera NIOS-PROKIT-1S40 FPGA development kit [51].

it available to the back-end and feeds the reference input of the LO synthesizer (6). The LO tone is split into three beams through (4) in order to coherently downconvert the RF signals coming from the three antenna inputs. The three I and Q BB pairs are passed to the back-end.

D. Back-End

The back-end is distributed on a shelf that fits in the 19-in rack, as shown in Fig. 5. The analog I and Q BB pairs pass through a low-pass filters (LPF) bank (8). The LPF's cutoff is 8 MHz. The filtered signals further feed the one-bit A/D conversion subsystem (9), which outputs a six-bit bus with the one-bit digitized I and Q signals. A ribbon cable drives the aforementioned bus to the signal processor (12). The signal processor is based on a field-programmable gate array (FPGA) development kit. It has been programmed to allocate all the signal-processing capabilities explained in Section IV. The signal-processor 40-MHz clock enters the back-end through the *Clock-in* signal, which comes from the front-end (see Fig. 4). This clock signal is split in two. One beam feeds the clock input of the FPGA (12), and the other is passed through a four-to-one frequency divider (10). Its output is a 10-MHz sinusoidal tone, coherent with the input 40-MHz 3.3-V CMOS square signal. This 10-MHz tone feeds the GPS receiver (11) which tracks all the satellites in view via antenna input 1, derived from the front-end. The GPS receiver continuously steers the 40-MHz system clock in the back-end (see again Fig. 4) through the *Frequency adjust* signal output. Done this way, the signal processor (12) can assume perfect knowledge of the GOLD-RTR instrument clock frequency with respect to the GPS time frame. The GOLD-RTR products, real-time computed waveforms, are sent from the signal processor to the laptop through the Ethernet cable.

E. Power Supply

The power supply is linear and not switched in order to avoid possible spurious interference with the very weak GPS signals. It provides the necessary 12-, 9-, 5-, and 3.3-V dc voltages.

IV. SIGNAL PROCESSOR

The design was burned onto an Altera Stratix EP1S40 FPGA chip [51]. It was configured to allocate 640 single-lag complex correlators and all the necessary control and monitoring electronics for programming and use. The number of correlators implemented is limited by the FPGA resources. The signal-processor design is modular and fills about 84% of the FPGA hardware resources.

A. Architecture

The main building blocks of the signal processor are shown in Fig. 6. The 40-MHz clock signal drives all the building blocks of the signal processor: registers, counters, memories, and microprocessors. The three BB I and Q pairs coming from the A/D stage are latched to a six-bit register at the 40-MHz clock rate; this register functions as the A/D sampling device because the sign extractors in the A/D stage (MAX961, see Fig. 5) actually run freely without clock intervention. After sampling, the bus of six BB one-bit signals is split into ten equal copies, which are input to the ten correlation channels. Each correlation channel contains 64 single-lag correlators in order to provide 64-lag waveforms at ~ 50 -ns spacing. The microprocessor labeled $\mu P1$ is responsible for receiving information

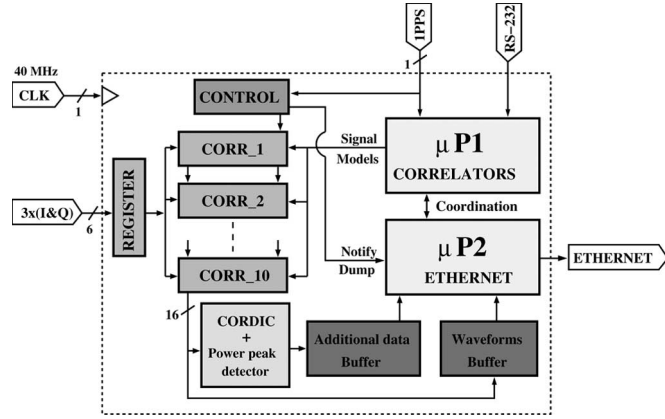


Fig. 6. Signal-processor block diagram. Its core is composed of ten correlation channels, each containing 64 single-lag correlators and computing, in parallel and in real time, 64-lag waveforms. Microprocessor $\mu P1$ programs each correlation channel with the appropriate signal models for cross correlation against the input signals. Microprocessor $\mu P2$ picks up the real-time computed waveforms and sends them to the external laptop via Ethernet.

about the GPS satellites in view from the GPS receiver and through the RS-232, in order to compute the appropriate signal models for cross correlation. Every second, the GPS receiver issues a second mark through the 1PPS signal. This is used by microprocessor $\mu P1$ as an interrupting signal asserting the arrival of a new data burst through the RS-232. Immediately after, and in accordance with the observation plans indicated by the user, $\mu P1$ computes the signal models that will be used by each correlation channel during the *next* second. When $\mu P1$ is performed with the computations, it loads the signal models (actually, the few parameters that completely define them) to small internal buffers in the correlation channels. These buffers allocate the signal model parameters until completion of the present second. As soon as a new 1PPS mark arrives, the correlation channels' control block (simply labeled *control* in Fig. 6) resets all the correlation channels to zero and orders them to load the signal model parameters from the aforementioned buffers. These two actions are performed in just one clock cycle, following the 1PPS mark. During the remaining 39 999 999 clock cycles for completion of this new second, each correlation channel internally runs the signal models for the full second. Summarizing, microprocessor $\mu P1$ follows a 1-Hz routine that involves: 1) receiving data through RS-232; 2) computing the signal model parameters; and 3) loading them to each of the ten correlation channels. The control block serves two main functions. One is to reset the correlation channels and order them to load the signal model parameters at a 1-Hz cadence (as mentioned). The other is to make the correlators integrate-and-dump at a rate of 1 kHz: starting from the second clock cycle after a 1PPS mark, it orders the correlators to start integrating for 39 300 contiguous clock cycles; at completion, a serial dumping of the correlator computed data is performed during 640 clock cycles. During the remaining 60 clock cycles (to complete the 40 000-clock-cycle integration period, 1 ms of time), the correlation channels are idle. This routine is performed 1000 times per second, so that each correlation channel computes one thousand 64-lag waveforms per second. Each millisecond, the real-time computed waveforms are se-

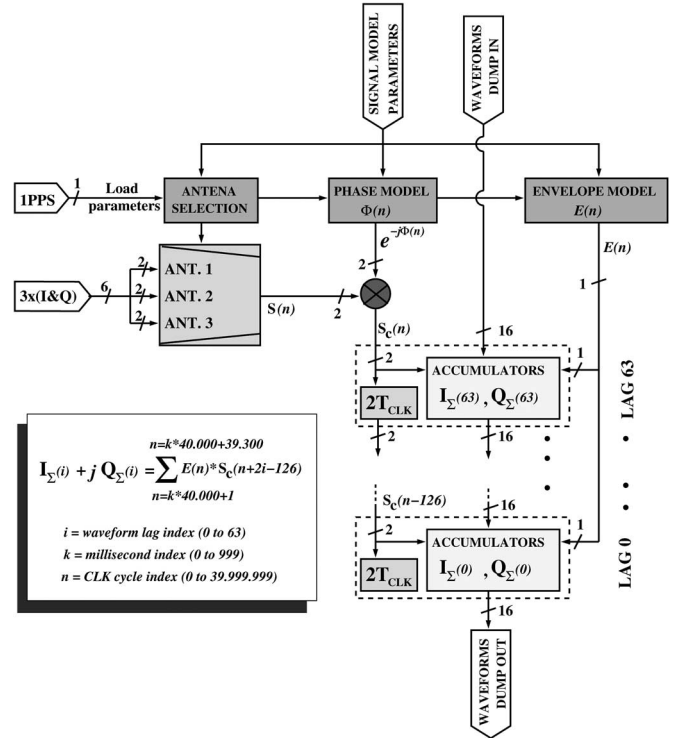


Fig. 7. Detailed block diagram of a correlation channel. Each of the 64 single-lag correlators are labeled accumulators. The phase- and envelope-model blocks are special digital hardware that, with the appropriate loading of the signal parameters, automatically compute the envelope and phase signal models for a full second. After counterrotation, a cascaded delay line of 64 lags simultaneously provides 64 delayed replicas of the counterrotated signal $S_c(n)$. After multiplication with the envelope signal model $E(n)$, the resulting 64 signals are accumulated over almost 1 ms. The resulting 64 complex signal pairs $[I_{\Sigma}(i), Q_{\Sigma}(i)]$ correspond to 64 I and Q samples of the cross-correlation function between the input signal and its model.

rially dumped to the *waveforms Buffer*. During dumping, the opportunity is taken to compute additional parameters for each waveform: the index corresponding to the lag with the greatest amplitude (it ranges from 0 to 63), the value of this amplitude, and the phase (from 0° to 360°) corresponding to this lag. This is achieved using specialized hardware that implements an eight-stage pipelined *CORDIC* processor [52] and a *maximum detector*. The *CORDIC* processor, with only shift-and-add operations, counterrotates each waveform lag toward the real axis and computes its phase. The maximum detector selects, from each waveform, the lag with the greatest amplitude and its corresponding phase. The final three parameters for each waveform are stored into the *Additional data Buffer*. This is performed entirely during the 640-clock-cycle dumping phase every millisecond. After a dumping is complete, the *control* block notifies microprocessor $\mu P2$, which immediately picks up the ten waveforms and the corresponding additional data, which it then sends via Ethernet to the laptop. This is done in less than 1 ms. Details of the different subblocks that form a correlation channel are shown in Fig. 7. The *phase model* and *envelope model* blocks are specialized hardware that automatically run, for a full second, the cross-correlation signal model. Both blocks have special programming input buffers that preallocate the signal model parameters coming from microprocessor $\mu P1$, as mentioned previously. The *antenna selection* block is simply

a latch that stores a value which indicates which of the three I and Q BB pairs feeding the input multiplexer is selected as a signal source. The signal on output of the multiplexer is a sequence of complex-valued samples, expressed as $S(n) \equiv I(n) + j \cdot Q(n)$. Each sample of this sequence has two bits that represent, respectively, the sign of the I and Q components of the analytic BB signal. Hence, $S(n)$ can only take the following four values: $\{1 + j, -1 + j, -1 - j, 1 - j\}$. The index n represents the clock cycle number after the last 1PPS mark. It ranges from 0 to 39 999 999 since the system works at 40 MHz. At this point, the sequence $S(n)$ is counterrotated by the counterrotation phasor model $e^{-j\Phi(n)}$ in order to completely remove the residual frequency of the signal due to the LO residual (300 kHz) plus the Doppler shifts (much smaller than 300 kHz). This counterrotation phasor is only codified with two bits. It is arranged in order to take one of the following values: $1, j, -1, -j$. In doing so, the counterrotated signal $S_c(n)$ takes values with in the same range as $S(n)$ and can still be codified with two bits. The counterrotation phasor is clearly a square signal, which contains the desired phasor tone of around 300 kHz, but also several higher order harmonics at integer multiples of the fundamental frequency. The higher order harmonics are undesired because they produce spurious downconversions at multiples of the fundamental frequency, which are present in the $S_c(n)$ signal. However, these are completely filtered out below the noise in the further 1-ms integration, which is 1-kHz low pass. The described arrangement is similar to the one used in the TurboRogue GPS receiver [37] and is designed to minimize the need for digital hardware resources. After counterrotation, the remaining $S_c(n)$ signal is ready for cross correlation. This signal is delayed through a 64-lag pipeline. Each lag corresponds to a delay of *two* clock cycles, with the clock cycle being the inverse of 40 MHz. In doing so, the 64 signals $S_c(n), S_c(n-2), S_c(n-4), \dots$, up to $S_c(n-126)$ are simultaneously available. All these signals are simultaneously multiplied by the envelope model $E(n)$ (the GPS C/A code replica of the satellite to be observed) and separately accumulated over a period of nearly 1 ms. There are two accumulators for every delayed replica of $S_c(n)$, for both the I and Q components. Since the envelope model is codified with one bit, the resulting I and Q components after multiplication by $E(n)$ are still represented by one bit, respectively. In fact, each accumulator is a 14-bit up/down binary counter, whose up/down control input is driven by either the I or Q mentioned signals after multiplication. Every millisecond k , the block that controls the correlation channels (see Fig. 6) resets the counters and then immediately enables them during a 39 300-clock-cycle period (0.9825 ms). During this period, for every clock cycle, the counters count up or down, depending on the signal present at its up/down control input. After the 39 300 cycles, integration is done, and each counter contains the I_Σ and Q_Σ components of each of the 64 lags of the waveform. The results are directly codified in two's complement. In order to rapidly dump the 640 (I_Σ, Q_Σ) pairs that have been simultaneously computed within each correlation channel and minimize hardware needs, a shifting strategy is used. Each of the two counters that form a single-lag accumulator has a synchronous load input, so that it can be loaded with an external value. This means that the

output of a single-lag accumulator is the input to the *next* single-lag accumulator, forming a chain of 640 lags. As soon as accumulation is complete, shifting is started by enabling the synchronous load input of all the accumulators. With 640 clock cycles, the 640 correlation results are dumped. After that, 60 clock cycles of spare time occur, and then, the process starts again. This routine is repeated 1000 times a second. It is worth mentioning that not all the 14 bits of each counter are retrieved, but just the eight most significant bits (MSBs) and the six least significant bits (LSBs) are left out. The noise power added in this quantization process is much lower than the Gaussian background thermal noise. Accordingly, in Fig. 7, the input–output waveform chains are shown with a 16-bit bus. The equation that appears in the said figure shows exactly how each waveform lag i is computed at each millisecond k .

B. Signal Models

The signal models used in the real-time cross-correlation process, automatically generated in the *Phase Model* and *Envelope Model* dedicated digital hardware blocks (see Fig. 7), have been designed so as to: 1) be valid for 1 s and 2) have the total accumulated mismodeling errors due to truncation to not exceed more than 2 mm during this period. In order to achieve both goals, the models consider the transmitted signal structure, the characteristics of both transmitter and receiver clocks, and propagation delay. Each GPS satellite has its own free-running clock, based on a high-stability (atomic) frequency standard. The GPS time scale, that will be denoted as t , is implemented by atomic clocks in the GPS ground control stations and the GPS satellites themselves. Since t is the result of a joint computation of all these clocks, none keeps the GPS time scale. As a result, every GPS satellite's clock has a bias with respect to t , which is constantly changing. Although the rate of change may be very small, in the order of 10^{-11} every second or less, this accumulates with pass of time offsets that may become as large as several hundred microseconds. To this offset, the user must add an additional relativistic clock offset, as the satellite moves with respect to the GPS receiver. The result is the transmitter satellite clock bias $b_{\text{TX}i}$. According to [33], the time scale $t_{\text{TX}i}$ kept by the i th GPS satellite clock (with PRN number i) can be related to the GPS time scale by the following expression:

$$t_{\text{TX}i} = t + b_{\text{TX}i} \quad \text{where} \quad b_{\text{TX}i} = b_{\text{TX}i}(t). \quad (1)$$

The user may accurately compute the value of $b_{\text{TX}i}$ because it is transmitted within the GPS broadcast message. As explained in Section III-C, the GOLD-RTR receiver 40-MHz clock is constantly steered toward GPS time. This ovenized crystal oscillator clock (OCXO) has an Allan variance of $5 \cdot 10^{-11}$ over a 1-s period, valid for external temperatures ranging from 0° to 70° . The steering process is very smooth, in order to avoid any loss of the clock's intrinsic stability: The OEM4-G2L GPS receiver [49], [50] adds a very slight voltage change to the *Frequency Control* signal once every 31 s (see Fig. 3). With everything arranged this way, it is guaranteed that the GOLD-RTR clock will not advance or delay the GPS time more than

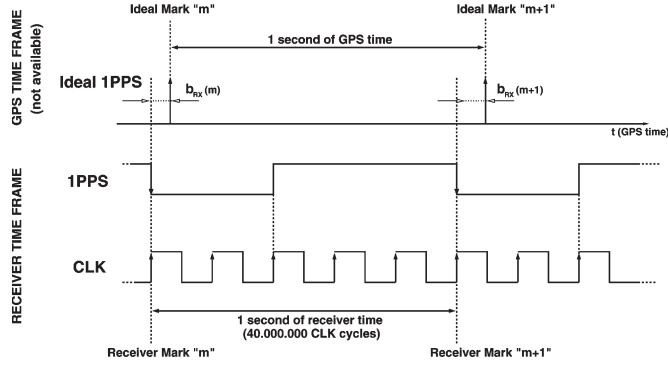


Fig. 8. Relation between the GPS time reference and the navigation receiver time. The former is represented at the top, where a second mark is issued for every second of GPS time. This is labeled as the ideal 1PPS signal, as this signal's availability would be desirable at the receiver end. Since it is never available, the receiver has its own 1PPS timing signal instead. The 1PPS signal is hardware-tight (coherent) to the receiver 40-MHz clock (CLK) so that it exactly issues a second mark every 40 000 000 clock cycles.

$1 \mu\text{s}$ at any moment. This time-offset error was not selected by the authors of this paper, but is the result of the clock-steering process made by the particular GPS navigation card, which was calibrated to handle an ovenized clock with the aforementioned stability characteristics. Shorter time offsets in the order of nanoseconds are achieved through performing a rougher and faster steering process, but this only makes sense when using clocks with poorer frequency stability such as a crystal oscillator (XO) or a thermally compensated XO (TCXO). This steering process is useful in two ways: 1) The receiver clock is close to the GPS time at an error of less than $1 \mu\text{s}$, which permits very precise georeferenciation of the real-time computed waveforms when performing experiments from a mobile flying platform (see Section VII); and 2) keeps the receiver real rate very close to its nominal rate (40 MHz) with respect to the GPS time, with a relative error near 10^{-10} . This last issue is accomplished through the use of an OCXO; with an XO or TCXO, it would not be as effective. As a consequence of the described arrangement, the GOLD-RTR clock t_{RX} can be expressed in terms of the GPS time t , with an expression analogous to (1)

$$t_{\text{RX}} = t + b_{\text{RX}} \quad \text{where} \quad b_{\text{RX}} = b_{\text{RX}}(t). \quad (2)$$

This formal relation is graphically represented in Fig. 8. The receiver's 1PPS signal issues the receiver's time second marks, which are offset with respect to GPS time by b_{RX} seconds, and this changes with time. The rate of change of this clock bias is what limits the relative deviation of the receiver's clock real rate with respect to its nominal value to 10^{-10} , measured with respect to t . The 1PPS signal is derived from the GPS receiver clock signal using a binary digital counter, which gives an output mark every 40 000 000 counts. Clearly, both signals are coherent (synchronous in the terminology of digital electronics). This is an important underlying assumption, as all the digital electronics in the GOLD-RTR back-end are driven by this clock. According to (1) and (2), the transmitter time frame can be expressed as a function of the receiver time frame

$$t_{\text{TX}i} = t_{\text{RX}} + (b_{\text{TX}i} - b_{\text{RX}}). \quad (3)$$

The navigation signal transmitted by the i th GPS satellite can be generically expressed as

$$S_{\text{TX}}^i(t), \quad i\text{th GPS satellite TX signal}. \quad (4)$$

The transmitted signal is propagated toward the GOLD-RTR receiver antennas either through the direct or reflected path (see Fig. 1). The delay suffered through propagation can be expressed as τ_i . It is defined as the time it takes the signal to travel from the transmitter antenna at time of transmission to the receiver's front-end at time of reception. Note that, this includes the free-space delay plus both the tropospheric and ionospheric delays and even the receiver-antenna downlink-cable delay. The signal received at the GOLD-RTR front-end, expressed in terms of receiver time t_{RX} , can be written as

$$\begin{aligned} S_{\text{RX}}^i(t_{\text{RX}}) &= S_{\text{TX}}^i(t_{\text{TX}i} - \tau_i) \\ &= S_{\text{TX}}^i(t_{\text{RX}} - [\tau_i + b_{\text{RX}} - b_{\text{TX}i}]) \end{aligned} \quad (5)$$

where the relation in (3) has been used. By definition, the delay that appears between square brackets on the right of the previous equation is the so-called *pseudorange*. This is one of the measurements performed by a GPS receiver when tracking a signal. It is normally expressed in meters

$$\rho_i = c_o \cdot (\tau_i + b_{\text{RX}} - b_{\text{TX}i}) \quad (6)$$

where $c_o \equiv 299\,792\,458 \text{ m/s}$ is the speed of light in vacuum as defined in the WGS-84 geodetic reference system used in GPS. The pseudorange is the signal delay as observed in the receiver front-end, *within* the receiver's time frame. Due to both transmitter and receiver clock biases, the pseudorange measurement ρ_i is clearly biased with respect to τ_i , which is the desired measurement for navigation (positioning) purposes. However, the ultimate purpose of the signal processor inside the GOLD-RTR is not radionavigation, but merely the computation of sampled versions (waveforms) of the cross-correlation function of the incoming GPS C/A L1 signals against their models, around the correlation peak. The accurate C/A code alignment information that this task requires, i.e., the *apparent* signal delay as seen from the receiver, is exactly contained in ρ_i . A typical GPS receiver tracks the direct signals received from all the satellites in view. The term *track* involves the continuous measurement of ρ_i and its rate of change due to the apparent radial velocity between the transmitter and receiver. This last parameter is directly related to the Doppler frequency measurement f_{D_i} by

$$\begin{aligned} \frac{\partial \rho_i}{\partial t_{\text{RX}}} &= -\lambda_{L1} \cdot f_{D_i}(t_{\text{RX}}) \quad \text{where} \\ \lambda_{L1} &= \frac{c_o}{f_{L1}}, \text{ the L1 wavelength} \\ f_{L1} &= 1\,575\,420\,000 \text{ Hz, the L1 carrier}. \end{aligned} \quad (7)$$

Strictly, the previous equation is an approximation since ionospheric dispersion causes the changes in pseudorange to slightly deviate from the carrier Doppler shift. However, the error introduced for this approximation is rather small for

short-term extrapolations [see (8) below]. In *GOLD-RTR*, the signals received through the up-looking antenna are continuously tracked by the *OEM4-G2L GPS* navigation receiver card. An external user can request the f_{D_i} and ρ_i measurements from that card through data logs. Each data log contains the aforementioned measurements for each of the GPS satellites being tracked plus a time-tag indicating the moment at which these measurements correspond. This time-tag is expressed in the receiver's time frame units: t_{RX} . This is a good match with the purpose of having an appropriate signal model, since at the receiver-end, everything is observed within the receiver time frame t_{RX} . Looking back into (5) and (6), it is clear that all that is required to complete the model of the received signal is

- 1) a model of S_{TX}^i , the transmitted GPS L1 signal [33];
- 2) a continuous knowledge of $\rho_i(t_{RX})$.

The signal processor achieves requirement 2) by requesting data logs from the GPS receiver once per second. The obtained measurements correspond to the 1PPS second marks, i.e., the times where t_{RX} takes integer values, denoted by the integer variable m (see Fig. 8). Since the required information is not available continuously, but in samples at a rate of 1 Hz, a time extrapolation of the $\rho_i(m)$ samples is required. This is accomplished through Doppler integration (7). At any moment Δt after the 1PPS mark ($t_{RX} = m$), the pseudorange values can be expressed as

$$\rho_i(m + \Delta t) = \rho_i(m) - \lambda_{L1} \cdot \int_{u=m}^{u=m+\Delta t} f_{D_i}(u) du. \quad (8)$$

The preceding expression indicates that a precise knowledge of the Doppler is necessary. Fortunately, it is available as 1-Hz measurements as well; once again, extrapolation is needed. In this case, an assumption of linear evolution is very good for a 2-s extrapolation period, since the Doppler variation in 1 s, $\Delta f_{D_i}(m)$, is in the order of 1 Hz/s, as observed from a low-dynamics (neither acrobat nor fighter) aircraft, and the second derivative can be ignored

$$\begin{aligned} f_{D_i}(m + \Delta t) &= f_{D_i}(m) + [f_{D_i}(m) - f_{D_i}(m - 1)] \cdot \Delta t \\ &= f_{D_i}(m) + [\Delta f_{D_i}(m)] \cdot \Delta t. \end{aligned} \quad (9)$$

It is important to note that a 2-s extrapolation period is needed because microprocessor $\mu P1$ (remind Fig. 6) receives the $\rho_i(m)$ and $f_{D_i}(m)$ measurements *after* the 1PPS mark m . It uses this information to compute the signal models that will be valid for the next second between marks $m + 1$ and $m + 2$. This procedure is depicted in Fig. 9. Activity A involves the computation of the extrapolated pseudorange $\hat{\rho}_i(m + 1)$ and extrapolated Doppler $\hat{f}_{D_i}(m + 1)$ values by using (8) and (9). The Doppler first derivative $\Delta \hat{f}_{D_i}(m + 1)$ is assumed to be the same as $\Delta f_{D_i}(m)$. Using these values, $\mu P1$ starts activity B, which involves the computation of the few signal model parameters corresponding to the second between 1PPS marks $m + 1$ and $m + 2$.

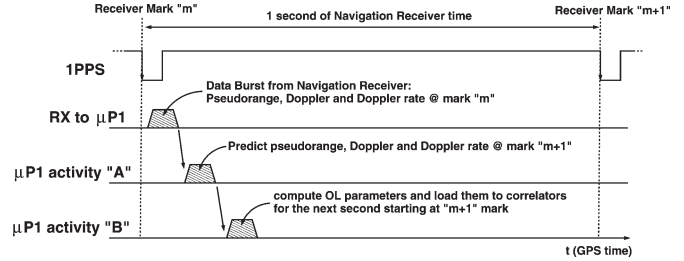


Fig. 9. Chronogram of the steady-state procedure performed by microprocessor $\mu P1$ in order to program the ten correlation channels with the appropriate signal model parameters. Every time there is a receiver time second mark, asserted by the falling edge of the 1PPS signal, microprocessor $\mu P1$ waits for the GPS satellites' related-data burst from the GPS receiver. As soon as all the data have been received (less than 100 ms after the 1PPS mark), $\mu P1$ starts activity A, which consists of predicting the pseudorange, Doppler, and Doppler rate for the next second mark $m + 1$, by using the previous pseudorange, Doppler, and Doppler rate measurements corresponding to mark m . With this predicted data, $\mu P1$ starts activity B, which consists of computing the OL parameters, i.e., the signal model parameters. When complete, these are loaded into each of the ten correlators. The correlators will use these model parameters between receiver marks $m + 1$ and $m + 2$ (the latter not depicted).

The signal model parameters are deduced by writing the model of the transmitted C/A L1 GPS signal in its analytic form

$$\begin{aligned} S_{TX}^i(t_{TXi}) &= e^{j(2\pi f_{L1} \cdot t_{TXi} + \phi)} \cdot E(a_{CR} \cdot t_{TXi}) \\ E(x) &\equiv \text{PRN}_i(\lfloor x \rfloor \bmod 1023) \\ \text{PRN}_i(u) &\text{ maps } u \text{ to the } i\text{th code chip value} \\ a_{CR} &\equiv 1.023 \text{ MHz, the C/A chipping rate} \end{aligned} \quad (10)$$

where the navigation bits are not taken into account; hence, they will be present as 180° random jumps in the phase of the computed 1-ms waveforms every 20-ms period. The function $E(x)$ assumes only the value $E(x) = \pm 1$ and represents the envelope of the signal as a periodic train of 1023 chips of the PRN spreading code of the i th GPS satellite. The function $\lfloor \cdot \rfloor$ takes the integer part of its argument. After propagation, the transmitted signal will be observed at the receiver-end, as indicated in (5). The analog RF front-end performs the direct I and Q downconversion. This is equivalent to counterrotating the received signal by the LO tone, represented by the $e^{-j(2\pi F_s \cdot M_b \cdot t_{RX})}$ exponential, where $F_s \equiv 40$ MHz is the reference clock frequency and $M_b \equiv 78\,756/2000$ is the LO synthesizer multiplication factor (see Fig. 4). The reference clock frequency has been labeled F_s because it is the sampling clock of the system, as mentioned earlier. So the BB analog I and Q received signal can be expressed as

$$\begin{aligned} S_{RX}^i(t_{RX}) &= e^{j(2\pi f_{L1} (t_{RX} - \frac{\rho_i(t_{RX})}{c_o}) - 2\pi F_s \cdot M_b \cdot t_{RX} + \phi)} \\ &\cdot E\left(a_{CR} \cdot \left(t_{RX} - \frac{\rho_i(t_{RX})}{c_o}\right)\right). \end{aligned} \quad (11)$$

We shall now substitute the pseudorange with its extrapolation expression (8) and implicitly (9) by considering the fact that we start the model with the values $\hat{\rho}_i(m + 1)$, $f_{D_i}(m + 1)$, and $\Delta \hat{f}_{D_i}(m + 1)$. Also, the receiver time should be substituted

with $t_{RX} = (m + 1) + \Delta t$. Taking the A/D sampling at the F_s rate into account, Δt will take the following discrete values:

$$\Delta t \equiv \frac{n}{F_s} \quad (12)$$

where n is the sample index starting at 1PPS mark $m + 1$, ranging from 0 to 39 999 999. By adequate manipulation and changing the integrals by summations (where $du = 1/F_s$), we obtain the discrete phase model, in cycles

$$\begin{aligned} \Phi(n) &= \text{constant} + C \cdot n + D \cdot n \cdot (n - 1) \\ C &\equiv \frac{f_{L1} + \hat{f}_{D_i}(m + 1)}{F_s} - M_b \\ D &\equiv \frac{\Delta \hat{f}_{D_i}(m + 1)}{2 \cdot F_s^2} \end{aligned} \quad (13)$$

and the x discrete model, in chips, which is used as the argument of $E(\cdot)$

$$\begin{aligned} x(n) &= \tau_o + A \cdot n + B \cdot n \cdot (n - 1) \\ \tau_o &\equiv \left(-a_{CR} \cdot \frac{\hat{\rho}_i(m + 1)}{c_o} \right) \\ A &\equiv a_{CR} \cdot \frac{f_{L1} + \hat{f}_{D_i}(m + 1)}{F_s \cdot f_{L1}} \\ B &\equiv a_{CR} \cdot \frac{\Delta \hat{f}_{D_i}(m + 1)}{2 \cdot F_s^2 \cdot f_{L1}}. \end{aligned} \quad (14)$$

The $E(\cdot)$ function, which assigns the correct chip value to its argument $x(n)$, is hardware implemented by merely selecting the correct PRN code corresponding to the i th satellite to be processed. Regarding (13), the initial constant is unimportant since the phase is never an absolute measurement. The digital hardware that runs the phase model is not actually reset to zero at every 1PPS mark, but starts with the phase of the last clock cycle before the 1PPS mark. Therefore, if a correlator is programmed to correlate the same satellite in consecutive seconds, the phase will not lose continuity. To summarize, when microprocessor $\mu P1$ ends activity B (see Fig. 9) in accordance with the user's requirements, it programs each correlation channel (see Fig. 7) by following three steps:

- 1) loads the antenna selection register with the desired value;
- 2) loads two registers in the *phase model* block with the C and D values;
- 3) loads four registers in the *envelope model* block; three with the τ_o , A , and B values, and a fourth register with the desired PRN number, corresponding to the i th satellite to be processed in that correlation channel.

At the beginning of this section, it was commented that the signal phase and envelope models, as expressed in (13) and (14), would not add more than 2-mm accumulated error due to truncation. In the phase case, this is translated into about 1/100th of a cycle, taking into account the fact that $\lambda_{L1} \equiv 190.3$ mm. For the $x(n)$ function case, as it is expressed in chips, this is translated into 1/150 000th of a chip since 1 chip = 300 m.

Since n takes values from 0 to 39 999 999, this is translated into the following precision requirements:

- 1) τ_o : (chips): 2^{-20} ;
- 2) A : (chips/sample): 2^{-44} ;
- 3) B : (chips/sample²): 2^{-68} ;
- 4) C : (cycles/sample): 2^{-32} ;
- 5) D : (cycles/sample²): 2^{-57} .

The digital hardware that runs automatically in each correlation channel, the phase and envelope models, has been implemented with the above binary precisions. Up to now, it has been assumed that the OEM4-G2L GPS receiver inside the GOLD-RTR delivered the correct ρ_i and f_{D_i} measurements for all the satellites in view; this is only true for the signals received through the direct ray, which are the only ones tracked by the GPS receiver, but not for the reflected ones (see Fig. 1). In this latter case, the signal processor assumes a simple geometric model that describes the additional propagation delay experienced by the reflected signal with respect to the direct one

$$\Delta \rho_i = 2 \cdot (H - U) \cdot \sin(e). \quad (15)$$

This simple model is accurate enough when flying in a vehicle at a low height above the geoid, in comparison with the radius of the Earth. H represents the height of the vehicle above the reference ellipsoid, as provided in real time by the GPS navigation receiver card, while U represents a user specified undulation, which is useful should the reflecting surface would not be at the reference ellipsoid level; e represents the GPS satellite's elevation as observed with respect to the local horizon, also provided by the GPS receiver in real time. In this situation, the sea surface is seen locally as a flat surface. It has also been assumed that the vehicle velocity vector is parallel to that surface, so that the Doppler of the specular point of the reflected signal is the same as the direct one. Therefore, when computing open-loop signal models for the reflected signals, the signal processor uses the same Doppler as for the direct signal,¹ and adds the additional (15) quantity to the direct signal's pseudorange measurement.

C. Correlators Schedule

The signal processor does not have any decision-making capacity in order to avoid uncontrolled actions. It programs each correlation channel *exactly* as the user requires. This is accomplished by means of a configuration file, which the user loads onto the signal processor via Ethernet by means of the graphical user interface (GUI) running on the laptop. The configuration file is a series of configuration lines. Each configuration line contains the following information:

- 1) a *time-tag* indicating the GPS week and second of the week at which the configuration line is first valid;
- 2) the following parameters repeated ten times to account for each of the ten correlation channels.
 - a) The *run/idle* flag, indicating whether the correlation channels have to be programmed or not. If idle, the signal processor does not send waveforms to the laptop.

¹ However, if the user forces an offset in the Doppler (see Section IV-C), then, this is added to the Doppler estimate in open-loop signal models.

- b) The *PRN* number of the GPS satellite to be processed. May range from 1 to 32 for normal GPS satellites, and as well as codes from 120 to 139 for GPS-WAAS satellites.
- c) The antenna *link* number that selects the GOLD-RTR antenna input used as a source signal for cross correlation. It ranges from 1 to 3.
- d) The *up/down* flag, indicating whether the model to be applied is up or down, as explained earlier (15).
- e) The delta frequency offset, ranging from -511 to 512 Hz, to force an offset in the Doppler. This directly affects parameters C and A of the open-loop envelope and phase signal models in (13) and (14).
- f) The *delta delay* offset, ranging from -1023 to 1024 m, to force an offset in the default pseudorange model. This directly affects parameter τ_0 of the open-loop envelope signal model in (14).
- g) The *undulation*, to consider the height of the reflecting surface with respect to the reference ellipsoid (15).

Not all combinations of the previous parameters are accepted. Particularly, the time-tags of each line must be consecutive, with a minimum separation of 1 s. Therefore, the correlators' configuration can be changed as often as once per second. Another restriction is the fact that, if a correlator is programmed with antenna link one selected, the up/down flag must be set to *up* since that antenna should always be up-looking. Flexibility is accounted for in the remaining parameter combinations. Section VII depicts some of these combinations. The preparation of a configuration file for an experiment requires prior knowledge of the following.

- 1) The precise time the experiment is going to start and stop.
- 2) Through what geographical points the instrument is going to move during the experiment, so as to order the signal processor to process the correct satellites. Should a correlator be programmed with a satellite that is not being tracked by the GPS receiver, the computed waveforms would be marked as *satellite not available*.

When the signal processor is loaded with a configuration file, it always compares its own time with the configuration file time-tags. If the time-tag of the first line of the file is for a time after the present moment, the signal processor waits until that moment. If it marks a time before the present, the signal processor moves its task pointer between lines, with time-tags indicating moments before and after the present moment. In whatever case, when the GPS time reaches the time-tag corresponding to each line, the signal processor programs (1 s in advance) the correlators with the user required configurations. Furthermore, it continues to program the correlators with such configurations until the GPS time reaches the time-tag of the next line.

D. Waveforms Data Format

If the signal processor is loaded with a configuration file, it will dump a set of ten data structures in every millisecond, each containing the 64-lag 1-ms waveform that was computed in real time in each correlation channel, plus additional data indicating the relevant correlation model parameters used and status flags. A C-expression describing this structure is depicted in Fig. 10.

```

struct waveform {
    int  weeksow;           // 0
    short millisecond;      // 4
    char status_numcorr;   // 6
    char link_updw;        // 7
    char prn;               // 8
    char max_pos;          // 9
    char amplitude;        // 10
    char phase;            // 11
    int  range_model;      // 12
    int  doppler_up;       // 16
    int  sampling_freq_int; // 20
    short sampling_freq_frac; // 24
    short d_freq;          // 26
    short d_delay;         // 28
    short sin_elevation;   // 30
    char data[128];        // 32
};                          // Total: 160 Bytes

```

Fig. 10. Waveform data structure declaration in C language. Those variables preceded by the mnemonic char use 1 B, those preceded by short use 2 B, and those preceded by int use 4 B. The structure begins with 32 B carrying several additional data parameters, and ends with an array of 128 characters carrying the 64 I and Q pairs of a 1-ms waveform, computed within a correlator (see Fig. 7).

The structure has 160 bytes. Those variables preceded by the mnemonic char use one byte, those preceded by short use two bytes, and those preceded by int use four bytes. The 32 leading bytes form a header carrying the additional data, while the DATA[128] character array carries the 64 lags corresponding to the 1-ms real-time computed waveform. Each lag is an I and Q pair, one byte for I and one byte for Q , respectively, codified in two's complement. The parameters in the header have the following meanings.

- 1) WEEKSOW and MILLISECOND is a time-tag, expressed in receiver time t_{RX} , of the moment at which the signal processor began to compute the waveform. For georeferenciation purposes it can be considered as GPS time, since the receiver time offset is always smaller than $1 \mu s$.
- 2) STATUS_NUMCORR indicates at what correlation channel the waveform was computed (1–10) and the status of the waveform. Status can be *OK*, *navigation bit*, and *satellite not available*. The first indicates that the data are correct. The second indicates that data are correct but there could be a jump of 180° in the phase during that millisecond, due to the navigation data modulation impinged in the navigation signal; it is better to ignore waveforms marked as such because this only happens once every 20 ms for GPS normal satellites (1–32). The last possible status indicates that the requested satellite to be processed was not tracked by the GPS receiver, so the waveform data is only noise.
- 3) LINK_UPDW indicates what antenna link (1–3) was used as a signal source for cross correlation and whether the model used was for direct signals (*up*) or for reflected signals (*down*), as explained in Section IV-B.
- 4) PRN is the PRN number of the processed satellite.
- 5) MAX_POS is the index of the waveform lag with greatest power.
- 6) AMPLITUDE of the waveform at the MAX_POS lag.
- 7) PHASE is the phase of the waveform at the MAX_POS lag.

- 8) RANGE_MODEL is zero if the model was *up* and takes the value indicated in (15) if the model was *down*.
- 9) DOPPLER_UP is the \hat{f}_{D_i} Doppler value delivered by the navigation receiver, corresponding to the direct signal of the indicated PRN number. This value, plus the D_FREQ value (see below) is the Doppler estimation used for crosscorrelation for both the up or down signals. This directly affects parameters C and A of the open-loop signal model [(13) and (14)].
- 10) SAMPLING_FREQ_INT and SAMPLING_FREQ_FRAC describe the sampling frequency (integer and fractional part), measured between 1PPS marks. This parameter is only kept for backward compatibility with previous versions of GOLD-RTR. This parameter always contains the 40 000 000 value, and the fraction is zero.
- 11) D_FREQ Doppler offset that was forced by the user and added to the Doppler frequency. This directly affects parameters C and A of the open-loop signal model [(13) and (14)].
- 12) D_DELAY delay offset forced by the user, that was added to the pseudorange. This directly affects parameter τ_0 of the open-loop signal model (14).
- 13) SIN_ELEVATION the sine of the satellite's elevation as seen on the local horizon.

When the GOLD-RTR is working, it dumps a stream of 1 600 000 bytes/s through the Ethernet. This flow is sinked by the laptop, which stores the real-time computed waveforms in several files. The total amount of data that can be stored is limited only by the capacity of the laptop's hard disk drive.

V. MACHINE-USER INTERFACE

The GOLD-RTR instrument is controlled through a GUI running on the laptop. A screen shot of this application is shown in Fig. 11. The GUI provides the following.

- 1) The *GOLD-RTR status* is a blinking text label to provide a way of monitoring the health of the instrument, indicating whether the instrument status flags are continuously received via Ethernet or not.
- 2) *GPS satellite availability* to show the PRN number as well as the received C/N_0 for all the GPS satellites tracked by the GPS receiver. The GPS time and date are also displayed.
- 3) *User action buttons*, divided between *test* and *experiment* actions. In both cases, the *configuration* button indicates the directory where the waveform data has to be stored and the path of the configuration file containing the correlation actions indicated by the user. The *test* action automatically performs a test, which consists of an automatically generated experiment of several seconds for checking purposes. The results are graphically displayed at the end of the test. The *start* action loads the instrument with the user-specified configuration file. The button then changes its label to *stop*, so that the user can abort the experiment before the scheduled time.
- 4) The *log register* provides logs of user actions as well as automatic actions performed by the GUI.

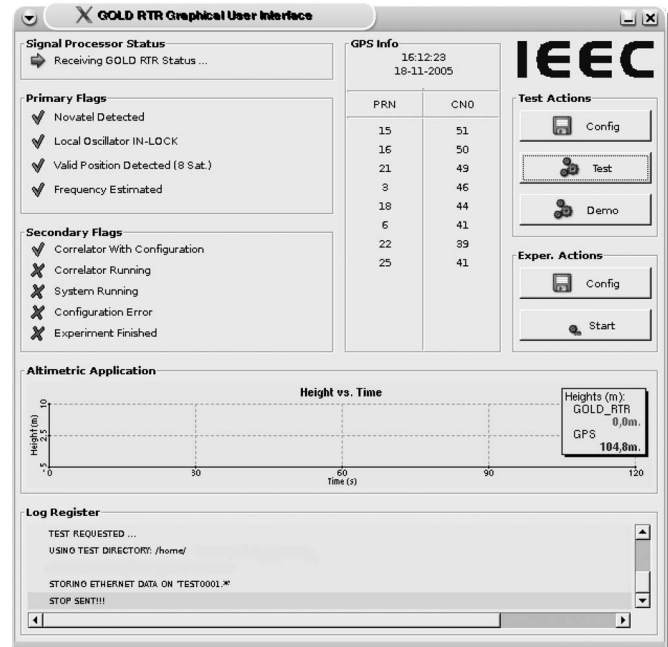


Fig. 11. Screen shot of the GOLD-RTR GUI, running on the laptop (see Fig. 2). The interface provides: 1) status of the GOLD-RTR (top left); 2) availability of GPS satellites (top center); 3) instrument controls (top right); 4) actions log register (bottom); and 5) real-time altimetric application graph (above the log register).

- 5) The *altimetric application* graph is a real-time application that uses GPS-R signals to determine the height of the up-/down-looking pair of antennas with respect to the reflective surface.

VI. LABORATORY READINESS TESTS

In order to check the correctness of the signal models generated by the signal processor (see Section IV-B), a controlled laboratory test was performed, in which there was strong knowledge of the signals gathered by the GOLD-RTR instrument. This was accomplished by using a SPIRENT GPS simulator test-bench. This comprised an NTNE10BA version (L1 only) STR4760 signal generator hardware platform and the SimGEN software running on a personal computer. This simulator provides an RF output signal that contains the same L1 GPS signals that would be observed in the output port of a receiving GPS antenna, as if moving in the real scenario being simulated. The STR4760 hardware platform provides a way of generating such a signal mixture, while the SimGEN software performs all the calculations to run the simulation and controls the STR4760 in order to generate the GPS signals accordingly. In order to emulate a real scenario with a static position, SimGEN only requires the corresponding GPS satellites' constellation almanac data in YUMA format, and the x - y - z ECEF coordinates of the antenna position. The test was designed to reproduce the true-scenario conditions in which waveform data had been experimentally collected beforehand with the GOLD-RTR instrument. The experiment was conducted on 41.4° N, 2.1° E, about 300 m above mean sea level, and data were recorded on March 23, 2005, beginning at 15 h, 23 m, and 0 s. The site was on the top of a hill, with full visibility of the

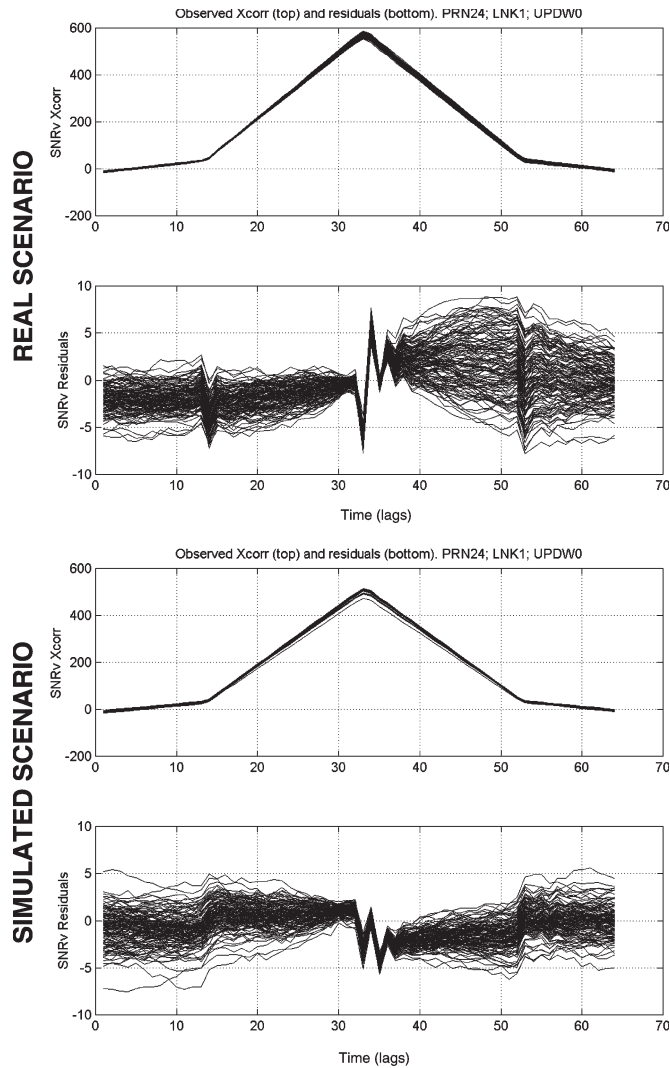


Fig. 12. Comparison of waveforms for satellite PRN 24 obtained in (top) a real field scenario and the same waveforms obtained when the GOLD-RTR was working under (bottom) a SPIRENT GPS simulator test bench that emulates that scenario. The signals gathered in the real scenario were uncontrolled, always in the presence of multipath, while the signals gathered in the GPS SPIRENT test bench were totally controlled, without multipath. Each graph depicts 120 s of 1-s integrated waveforms and the residuals of these waveforms after subtracting the best-fit of its model around the peak.

whole zenith hemisphere, with no nearby metallic structures. A zenith-pointing choke-ring antenna was used. Despite of all these multipath-avoidance precautions and after 1-s integration (50 dB SNR), the collected waveforms still seemed to indicate the presence of a diffuse multipath, comparable to thermal noise power levels (see Fig. 12, real scenario). Since this was a very slight effect, doubts may have arisen about their true origin: real multipath or mismodeling errors in the cross-correlation signal models. If it was a mismodeling error, this has to appear in the simulated environment as well. If it was real multipath, the waveforms collected in the simulated environment should not show evidence of the described effects and should exactly match the corresponding PRN code autocorrelation, only corrupted by the presence of thermal noise. The laboratory test was performed on May 27, 2005. The STR4760 RF output was plugged to the GOLD-RTR up-looking antenna input. It

was loaded with the same configuration file as that used in the real scenario. This configuration file had only one line, with instructions for programming eight of the ten correlators to collect waveforms corresponding to the eight satellites that were in view on March 23, at that particular site. The test lasted 120 s, obtaining a total of 120 000 1-ms coherent integrated waveforms for every satellite. For both the real and simulated scenarios, the 120 s of real-time-collected data was further integrated up to 1-s periods, reducing the results to just 120 waveforms per satellite. A comparison of the results for both the real and simulated scenarios and for just one of the eight processed satellites is shown in Fig. 12. There are two graphs for each scenario. The top graph shows the 120 superimposed 1-s integrated waveforms. Only the I component is shown since the waveforms have been counterrotated toward the real axis. This process is necessary in order to correctly compare the real cross correlation with the theoretical infinite-bandwidth PRN code autocorrelation. The residuals graph is shown below the waveforms graph, depicting the superimposed differences between each waveform and its best-fit model. The model used is the exact theoretical PRN autocorrelation of that particular satellite. The delay fitting is performed by implementing an early prompt-late delay discriminator with three lags around the peak. The estimation of amplitude is taken to be that corresponding to the lag with the greatest power. The simulated scenario waveform data in Fig. 12 show that the 120 superimposed 1-s waveforms are structured evenly left to right with respect to the peak; the background noise rms power seems even. This is confirmed in the residuals, which show this even symmetry better. At the center of the residuals graph, the thermal noise is nearly zero because the method for estimating the time of arrival (TOA) works around the central lag. The noise power increases gradually from the center up to the edges of the triangle. These simulated-scenario results match the theoretical predictions, thus confirming that the signal models used in the signal processor are adequate. This confirms that the unevenness of the residuals in the real scenario is the result of diffuse multipath. In this latter case, the increase in the power of the residuals toward the right is a confirmation that a small fraction of back-scattered energy from the surrounding terrain was received with an additional delay.

VII. FIRST FLIGHT CAMPAIGNS

Two successful flights using a pressurized jet aircraft were performed on July 13 and 14, 2005, at ~ 9300 m above mean sea level and ~ 130 -m/s speed, flying over two different areas of the western Mediterranean. A total amount of 5 h of real-time data was collected, which corresponds to 180 million 1-ms waveforms (29 GB). The purpose of the flights was to check the instrument's performance for altimetric, scatterometric, and polarimetric applications. This was accomplished by loading the GOLD-RTR with several configuration files, which were consecutively loaded into the instrument during the flights by an onboard human operator. These files were prepared beforehand to test all the useful combinations with the parameters that control the cross-correlation models in each of the ten correlation channels: *up* or *down*, signal source link (1–3), forced

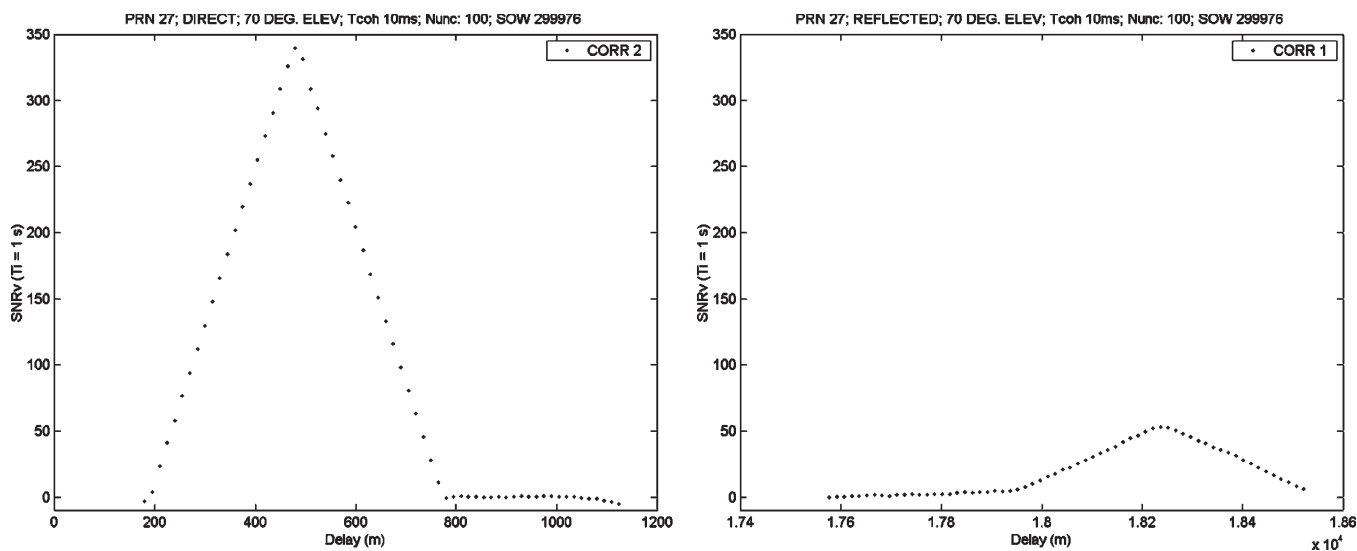


Fig. 13. (Left) Direct and (right) reflected 64-lags amplitude waveforms corresponding to PRN 27 1 s of integration time. The signal power was normalized to the background Gaussian noise power, so that the amplitude is expressed in SNR voltage units. The SNR peaks are 50.5 and 34.5 dB, respectively. Note that, the reflected waveform appears quite undistorted; this is because the sea was not too rough in the observed zone.

delay-offset, and forced Doppler-offset. This section provides samples of the real-time collected waveforms, which graphically illustrate some of the combinations tested, a sample of the real-time GNSS-R altimeter application that may be run under the GOLD-RTR GUI (see Section V) and preliminary measurements of the sea roughness.

A. Direct/Reflected Delay Maps

These measurements are obtained by using two correlation channels per PRN code, one for the up-looking right-hand circularly polarized (RHCP) antenna and the other for the down-looking left-hand circularly polarized (LHCP) antenna, up to five PRNs simultaneously. Therefore, the instrument computes and stores in the laptop disk ten complex-valued 1-ms waveforms per millisecond. Upon postprocessing, these waveforms are further integrated up to 1 s in order to achieve a higher SNR. A sample pair of direct/reflected 1-s waveforms is shown in Fig. 13. Since the signal models used in the real-time cross-correlation process are valid and accurate enough for periods of 1 s (see Section IV-B), the integration of the 1-ms waveforms up to 1-s periods does not require any time realignment of the 1-ms waveform lags prior to further postprocessing integration. The latter consists of the following.

- 1) The coherent summations of ten 1-ms waveforms (direct summation of complex-valued waveforms), which results in 10-ms coherent waveforms. The corresponding bandwidth for these 10-ms waveforms is 100 Hz.
- 2) The incoherent summation of 100 10-ms waveforms. This is accomplished by: 1) counterrotating each 10-ms waveform with the phase of the lag of greatest power and then taking only the real part of the resulting waveform and 2) performing a direct summation of the 100 real-valued resulting waveforms. This approach only works if the SNR at 10 ms is around 6 dB or greater, so that

the signal phase is properly estimated. But, it has the advantage that: 1) the resulting 1-s waveforms are corrupted only by Gaussian zero-mean noise statistics and 2) the waveform shape can be directly compared to the corresponding theoretical PRN code autocorrelation.

This approach opens the possibility of a linear resolution of the problem, i.e., trying to identify the sea reflection channel by comparing the direct and reflected waveforms, as a classical linear channel identification problem corrupted by zero-mean Gaussian noise. Note that, this would not be possible in the traditional incoherent integration method, which takes the square root of the power of each waveform lag, yielding: 1) a Rice nonzero-mean noise statistics that is parameterized by the signal's amplitude; and 2) a waveform shape that cannot be directly compared to the theoretical PRN autocorrelation because it has been distorted when taking the square root of each lag's power. The data acquired using this configuration showed that the reflected waveforms are correctly aligned with the direct ones according to the range model provided by the navigation card. This is a useful result since it indicates that the reflected-to-direct delay of the signals can be identically obtained with sole measurements of the reflected waveforms plus the RANGE_MODEL parameter (see Section IV-D) applied in the signal processor, with no need to occupy correlation channels to allocate the waveforms of the direct signals. Therefore, the GOLD-RTR is able to acquire altimetric data for up to ten satellites in parallel.

B. Doppler/Delay Maps

These measurements are obtained by using all the correlation channels with a single PRN code. We devoted the first channel to cross-correlate against the direct signal coming from the up-looking antenna (not necessary any more as discovered after the experiment and explained above), while the remaining nine

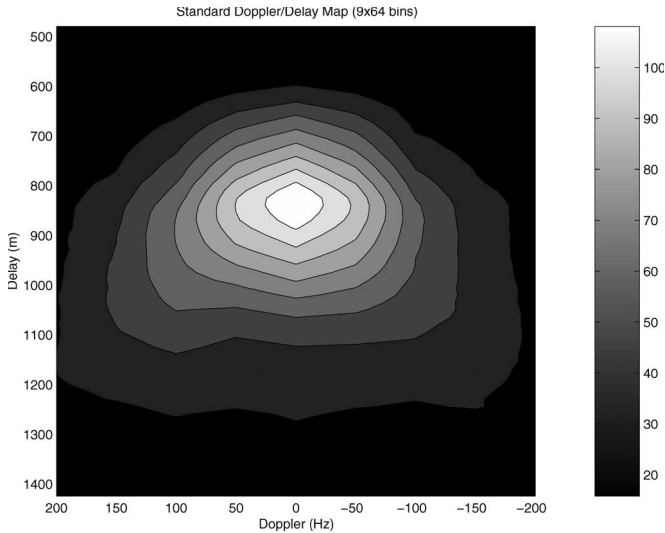


Fig. 14. Doppler/delay amplitude map (9×64 bins), corresponding to 1 s of data. The grayscalebar units are expressed in SNR voltage. This map has been computed by coherently integrating the 1-ms waveform products up to 10 ms and then incoherently integrating—by taking the square root of the power—up to 1 s. These observations were obtained by configuring the instrument with nine correlation channels cross correlating against the reflected signals and forcing Doppler offsets in the counterrotation phasor model from -200 to 200 Hz, in 50-Hz steps.

channels cross correlated against the reflected signals by forcing different frequency offsets in the signal model (D_FREQ in Section IV-D). A range of frequencies from -200 to 200 Hz, in 50-Hz steps, were selected. The further integration of the 1-ms waveforms is coherent up to 10 ms (then the bandwidth is 100 Hz) and incoherent up to 1 s. The incoherent integration is made by taking the square root of the power of each waveform lag (the classical method). The result is one Doppler/delay power map per second of the reflected signal data. A sample of such a map is shown in Fig. 14 as a grayscale-filled contour plot. The amplitude is expressed in SNR voltage after 1-s integration.

It is important to note that the roughly half-moon shape of the map matches the theoretical predictions: the energy reflected off the specular reflection point has the least delay and zero Doppler. As we move away from the specular reflection point, the scattered signal is always affected by an additional Doppler, and the propagation path is greater, providing an additional delay. Such a map can be used to sense the characteristics of the reflecting surface roughness and, indirectly, surface wind speed vectors (e.g., [53]).

C. Real-Time Coarse Altimetric Application

The GOLD-RTR instrument features a real-time coarse altimetric application that runs in parallel with the waveform storage application in the laptop. The altimetric application only runs if the GOLD-RTR has already been loaded through the demo or test actions buttons (see Fig. 11), with a configuration file that groups the ten correlation channels into five up/down pairs, each pair correlating against a single PRN (note that, from the results of the experimental data shown afterward, it is also possible to use the ten correlator channels to pick reflected signals, since the waveforms obtained are aligned ac-

cordingly to the known range model). Under these conditions, the altimetric application receives five up/down waveform pairs every millisecond. The application further integrates these 1-ms waveforms up to one second, yielding five high-SNR up/down waveform pairs. An example of such a waveform pair is shown in Fig. 13. Using this information, it computes five delay observables every second, i.e., the differences in TOA between the direct and reflected signals. This computation is made using an early-prompt-late estimator, with the underlying assumption that the reflected signal will be of the same shape as the direct one. Strictly, this is only true at very low altitudes or when the reflecting surface is almost flat.²

The following simple model is used in this application to relate the five delay observables $\Delta\rho_i$ with the aircraft height above sea level

$$\Delta\rho_i = 2 \cdot (H_{\text{MSL}}) \cdot \sin(e) + b_c. \quad (16)$$

The model has only two parameters: the aircraft height above mean sea level H_{MSL} and a constant bias b_c . This bias absorbs both the difference in the downlink-cable lengths between the down- and up-looking antennas, and the difference in the D_DELAY parameter set by the user between the down and up waveforms (see Section IV-D). The sine of the satellite elevation e above the local horizon is recorded in the waveform header (once again see Section IV-D). The estimation of the H_{MSL} and b_c parameters is made by performing a simple least squares fit of the model to the five delay observables. The result is a measurement of the aircraft height above sea level every second. The two flights performed on July 13 and 14 were mainly programmed for collecting scientific data. This was accomplished for almost all the time that the aircraft was flying at the same height. However, both the climb and descent phases of the flights were free. So, we took the opportunity in both flights to perform a coarse real-time altimetric test at the end of the flight during the descent. Graphical results corresponding the July 14 test are shown in Fig. 15. Only about 3 min is shown in order to clarify the precision of this GNSS-R passive real-time aircraft RADAR altimeter. In the top panel, the GNSS-R real-time aircraft height measurements (dots) are compared with: 1) the precise trajectory (solid line) of the aircraft and 2) the real-time height measurements provided by the Novatel OEM4-G2L GPS receiver card (dashed line). The precise trajectory of the aircraft is computed by the GPS standard fine postprocess, using the observables generated onboard by the GPS receiver card, and the precise *a posteriori* satellite orbits and clocks. This is considered the true trajectory. It should be noted that GPS-R measurements are single frequency (L1) and differential, while both the real-time and postprocess GPS positioning are dual frequency (L1 and L2) and absolute. In the bottom panel, a ground projection of the aircraft's trajectory is shown (solid line) during the mentioned descent phase and landing as well as the ground tracks of the specular reflection points (gray spots) of the GPS-R signals processed by the GNSS-R real-time coarse altimeter. The precision of the GNSS-R real-time height measurements is shown to be about 4-m rms before

²However, this application was only designed for demonstration purposes.

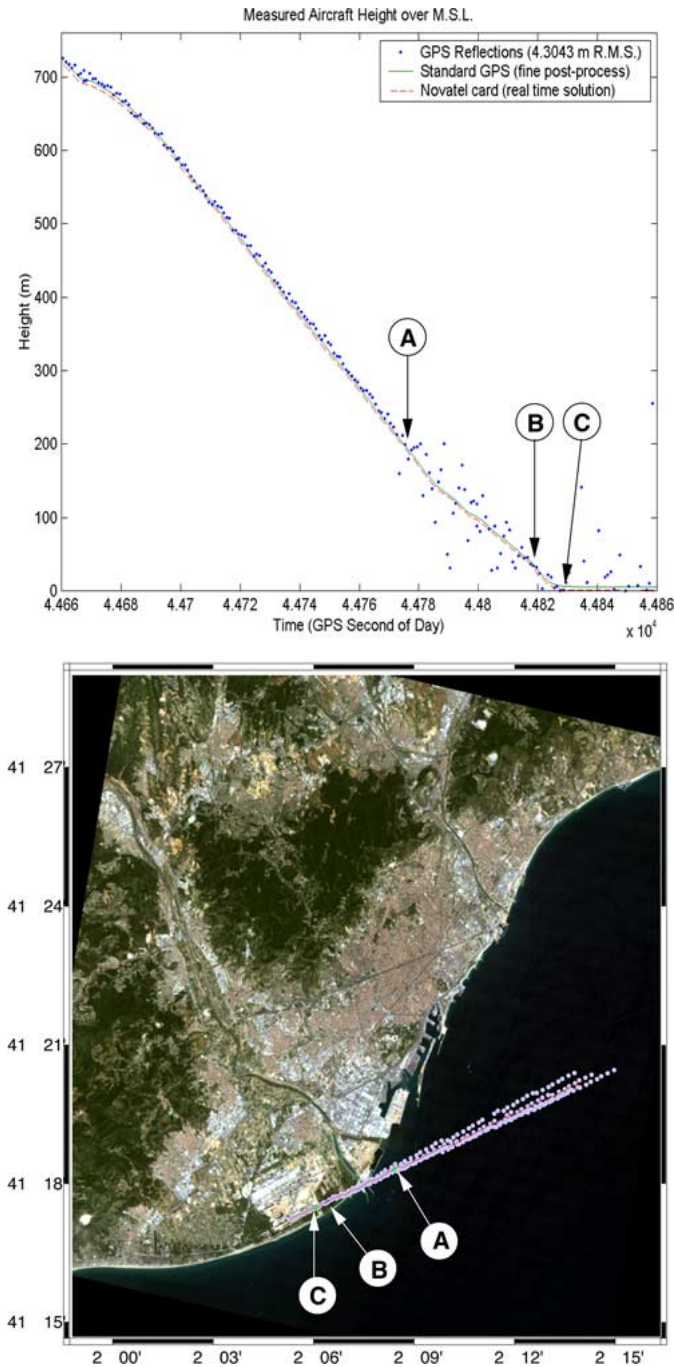


Fig. 15. (Top) Aircraft height measurements with respect to the sea surface, corresponding to the final descent phase and landing of the July 14, 2005 flight. The real-time coarse GNSS-R height measurements (dots) are compared with: 1) the precise trajectory (solid line) computed by the GPS standard fine postprocess methods, using the precise GPS satellite orbits and clocks and 2) the real-time height measurements provided by the Novatel OEM4-G2L GPS receiver card (dashed line). (Bottom) Ground projection of the aircraft's trajectory over the background image of the city of Barcelona during the aforementioned descent phase (solid line) and ground tracks of the specular reflection points (gray spots) of the GPS-R signals processed. Barcelona Landsat TM background image: ESA Copyright 2004. Distributed by Eurimage.

approaching point (A). This may be fairly coarse, but does however reasonably match the fact that, when using an Earth-bound omnidirectional GPS antenna for standard GPS positioning, the

accuracy of the envelope-based³ pseudorange observables after 1 s of integration (and using an early prompt-late estimator) is about 1 m rms. [54]. Apart from the direct signals, the altimetric application also deals with reflected signals. The reflected signals are affected by factors that degrade the SNR, such as the sea surface reflection coefficient (lower than one) and the sea surface roughness which distorts the signal shape. This effect worsens as altitude increases, introducing greater offsets in the determination of the reflected signal's delay. From point (A), the noise in the GNSS-R height measurements increases abruptly. This is probably due to the transition from sea to ground, where reflections may come from multiple directions and signal strength is reduced. Point (B) marks a short sequence of about 5 s, very near to the ground, where noise is reduced back again to the 4 m rms. During this phase, the aircraft flew over a natural protected zone that has a pond. Point (C) marks the landing time/place. This passive GNSS-R altimeter could be useful as an alternative to standard real-time GPS positioning, when used only for purposes of height determination. It has to be noted that the accuracy of real-time GPS positioning is affected by the precision of the real-time broadcast satellite ephemerides, which can induce position biases in the order of tens of meters. The dashed line in Fig. 15 is biased with respect to the solid line. The GNSS-R real-time altimeter presented here is independent of this (because it is differential) and could easily provide unbiased height measurements when flying at low altitudes.

D. Near-Real-Time Sea Surface Roughness

A set of algorithms has been designed and implemented for inverting delay waveforms into sea-surface-roughness estimates in a near-real-time pipe. Because of the low computing costs and the independence of this approach from postprocessed GPS products (such as precise orbits, transmitter clock corrections, or receiver trajectory), this algorithm could be integrated in the software part of the instrument to provide the mean-square slopes (MSS) of the sea surface. The technique is based on the nonlinear relationship between the supplementary delay suffered by the reflected waveform (shifting its peak location with respect to the optical reflected path delay) and the sea surface roughness statistics. In the past [6], a simplified model was used to relate the roughness driven delay and the effective (calibration requiring) MSS product. The approach has now been enhanced by using a complete integral model (absolute, no need of calibration) such as the one in [23], using the sea surface spectrum of [20]. The combined model provides the power waveform as a function of the geometric parameters and the surface MSS: $P^{\text{mod}}(\tau; \text{geometry}, \text{mss})$. The same peak-extractor operator used on the real data is used here to interpolate the delay of the maximum amplitude of the modeled waveform: $\Delta\rho_{\text{scatt}}^{\text{model}}(\text{mss}, \text{geometry}) = \text{PeakExtract}[P^{\text{mod}}(\tau; \text{geometry}, \text{mss})]$. The partial derivatives with respect to an *a priori* value of the mss (mss_0) are finally used to linearize the model: $[\Delta\rho_{\text{scatt}}^{\text{model}}(\text{mss}) - \Delta\rho_{\text{scatt}}^{\text{model}}(\text{mss}_0)] / [\text{mss} - \text{mss}_0]$. The iteration number depends on the quality of mss_0 . We applied this technique to the data obtained during the

³Not smoothed by the carrier phase

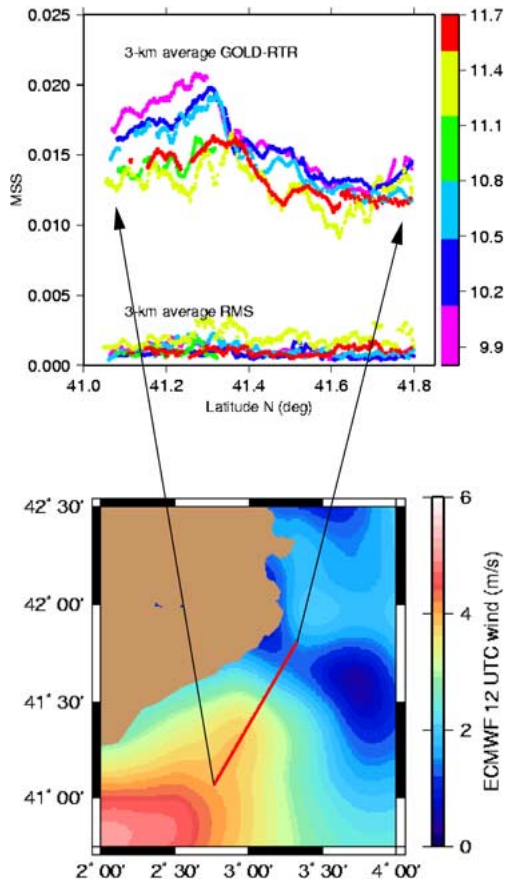


Fig. 16. (Top) MSS obtained with the near-real-time application and averaged at ~ 3 -km along-track resolution. The color scale stands for the time, in hours of the day (UTC). A clear north–south gradient of the surface roughness is detected, and some of its finer features are consistent along the repeated subsequent over passes. Moreover, the gradient is consistent with the wind speed reanalyzed by ECMWF (background color in bottom figure), where we have over plotted the trajectory of the craft (red line).

July 2005 flights. The resulting MSS, averaged within ~ 3 -km along-track resolution, is displayed in Fig. 16 (top) while the aircraft flew six times over an ~ 100 -km straight path for 2 h [Fig. 16 (bottom)]. The dispersion of the averaging process is small (< 0.001 on average), allowing the detection of features below a 10-km horizontal scale that are consistent along the different subsequent over passes. Furthermore, a north–south gradient of the MSS is identified, in qualitative agreement with the ECMWF reanalyzed wind product [Fig. 16 (bottom)]. Therefore, the GOLD-RTR potentially becomes a near-real-time instrument for providing L-band MSS of the sea surface.

VIII. SUMMARY

A technical description of the GOLD-RTR receiver has been presented, covering the hardware architecture and user interface of the instrument, its internal signal-processor architecture, and its signal-processing chain. All the relevant details have been explained for automatic real-time computation through ten independent correlation channels, each millisecond, of 64-lag complex-valued cross correlations between the input L1 C/A GPS signals and their models. The observations that can be

made with the GOLD-RTR receiver are highly flexible, making it possible to compute several synchronous delay maps for altimetry applications or Doppler/delay maps for scatterometry/polarimetric applications. The review of the instrumentation used previously in the field of Earth remote sensing using GPS-R clearly shows that the GOLD-RTR receiver provides a new and highly appropriate framework for the scientific user, who is mainly interested in extracting geophysical information from the waveforms, but not in computing the waveforms themselves. The GOLD-RTR provides a huge amount (compared to previous instruments) of automatically real-time computed waveforms immediately after an experiment, appropriately recorded in data structures, without the need of any effort from the user. The aim of the present paper is to provide an appropriate comfortable framework for the GPS-R community to perform thorough field campaigns and to noticeably speed up the study of GPS-R remote sensing techniques.

ACKNOWLEDGMENT

The authors would like to thank J. T. Badia and S. R. Vedrilla for their contributions in the assembly of the GOLD-RTR instrument hardware as well as their participation in the July 2005 flights, D. Pino (IEEC/UPC) for extracting the ECMWF products, The Centre Tecnològic de Telecomunicacions de Catalunya (CTTC) for providing access to their RF instrumentation several times during the development phase of the instrument, J. Torres and J. R. M. Romero from the Instituto Nacional de Técnica Aeroespacial (INTA) for facilitating the use of their SPIRENT GPS simulator, The Institut Cartogràfic de Catalunya (ICC) for computing the aircraft kinematic solutions and their pilots (Santi and Jordi) for the careful execution of the flight plans, and A. Hirschmann and D. Owen for checking the style of the manuscript.

REFERENCES

- [1] R. A. Simpson, "Spacecraft studies of planetary surfaces using bistatic radar," *IEEE Trans. Geosci. Remote Sens.*, vol. 31, no. 2, pp. 465–482, Mar. 1993.
- [2] M. Martín-Neira, "A passive reflectometry and interferometry system (PARIS): Application to ocean altimetry," *ESA J.*, vol. 17, pp. 331–355, Dec. 1993.
- [3] M. Martín-Neira, M. Caparrini, J. Font-Rosselló, S. Lannelongue, and C. S. Vallmitjana, "The PARIS concept: An experimental demonstration of sea surface altimetry using GPS reflected signals," *IEEE Trans. Geosci. Remote Sens.*, vol. 39, no. 1, pp. 142–149, Jan. 2001.
- [4] J. L. Garrison, S. J. Katzberg, and C. T. Howell, "Detection of ocean reflected GPS signals: Theory and experiment," in *Proc. IEEE Southeastcon Engineering the New Century*, Blacksburg, VA, Apr. 12–14, 1997, pp. 290–294.
- [5] S. T. Lowe, C. Zuffada, Y. Chao, P. Kroger, L. E. Young, and J. L. LaBrecque, "5-cm precision aircraft ocean altimetry using GPS reflections," *Geophys. Res. Lett.*, vol. 29, no. 10, 1375, May 2002.
- [6] A. Rius, J. M. Aparicio, E. Cardellach, M. Martín-Neira, and B. Chapron, "Sea surface state measured using GPS reflected signals," *Geophys. Res. Lett.*, vol. 29, no. 23, 2122, Dec. 2002.
- [7] G. Ruffini, F. Soulat, M. Caparrini, O. Germain, and M. Martín-Neira, "The Eddy experiment: Accurate GNSS-R ocean altimetry from low altitude aircraft," *Geophys. Res. Lett.*, vol. 31, no. 12, L12306, Jun. 2004.
- [8] K. Anderson, "A global positioning system (GPS) tide gauge," NATO Advisory Group for Aerosp. Res. Develop., Tech. Rep. CP-582, 1996.
- [9] R. N. Treuhaft, S. T. Lowe, C. Zuffada, and Y. Chao, "Two-cm GPS altimetry over Crater Lake," *Geophys. Res. Lett.*, vol. 28, no. 23, pp. 4343–4346, 2001.

- [10] M. Belmonte and M. Martín-Neira, "GNSS reflections: First altimetry products from bridge-2 field campaign," in *Proc. 1st ESA Workshop Satellite Navigat. User Equipment Technol. (NAVITEC)*, 2001, pp. 465–479.
- [11] M. Martín-Neira, P. Colmenarejo, G. Ruffini, and C. Serra, "Altimetry precision of 1 cm over a pond using the wide-lane carrier phase of GPS reflected signals," *Can. J. Remote Sens.*, vol. 28, no. 3, pp. 394–403, Jun. 2002.
- [12] M. L. Beekhuis, M. Belmonte, N. Bastarrachea, M. Martín-Neira, J. Torrobella, and O. Nogués-Correig, "Zeelandbrug III experiment, a GPS-R experiment with new GNSS-R receiver to retrieve geophysical parameters as sea surface roughness and sea level," in *Proc. Oceanography with GNSS Reflections Workshop*, Jul. 17–18, 2003, pp. 111–112. [Online]. Available: <http://starlab.es>
- [13] M. Caparrini, L. Ruffini, and G. Ruffini, "PARFAIT: GNSS-R coastal altimetry," in *Proc. Workshop Oceanography with GNSS Reflections*, Jul. 17–18, 2003, pp. 51–68.
- [14] E. Cardellach, C. O. Ao, M. de la Torre-Juárez, and G. A. Hajj, "Carrier phase delay altimetry with GPS-reflection/occultation interferometry from low Earth orbiters," *Geophys. Res. Lett.*, vol. 31, no. 10, L10402, May 2004.
- [15] J. L. Garrison and S. J. Katzberg, "The application of reflected GPS signals to ocean remote sensing," *Remote Sens. Environ.*, vol. 73, no. 2, pp. 175–187, Aug. 2000.
- [16] A. Komjathy, V. U. Zavorotny, P. Axelrad, G. H. Born, and J. L. Garrison, "GPS signal scattering from sea surface: Wind-speed retrieval using experimental data and theoretical model," *Remote Sens. Environ.*, vol. 73, no. 2, pp. 162–174, Aug. 2000.
- [17] J. L. Garrison, A. Komjathy, V. U. Zavorotny, and S. J. Katzberg, "Wind speed measurement using forward scattered GPS signals," *IEEE Trans. Geosci. Remote Sens.*, vol. 40, no. 1, pp. 50–65, Jan. 2002.
- [18] E. Cardellach, G. Ruffini, D. Pino, A. Rius, A. Komjathy, and L. Garrison, "Mediterranean balloon experiment: Ocean wind speed sensing from the stratosphere using GPS reflections," *Remote Sens. Environ.*, vol. 88, no. 3, pp. 351–362, Dec. 2003.
- [19] O. Germain, G. Ruffini, F. Soulat, M. Caparrini, B. Chapron, and P. Silvestrin, "Speculometry from low altitude aircraft," in *Proc. Oceanography with GNSS Reflections Workshop*, Jul. 17–18, 2003, pp. 107–110. [Online]. Available: <http://starlab.es>
- [20] T. Elfouhaily, B. Chapron, K. Katsaros, and D. Vandemark, "A unified directional spectrum for long and short wind-driven waves," *J. Geophys. Res.*, vol. 102, no. C7, pp. 15781–15796, Jul. 1997.
- [21] J. L. Garrison, S. J. Katzberg, and M. I. Hill, "Effect of sea roughness on bistatically scattered range coded signals from the global positioning system," *Geophys. Res. Lett.*, vol. 25, no. 13, pp. 2257–2260, Jul. 1998.
- [22] B. Lin, S. J. Katzberg, J. L. Garrison, and B. A. Wielicki, "Relationship between GPS signals reflected from sea surfaces and surface winds: Modeling results and comparisons with aircraft measurements," *J. Geophys. Res.*, vol. 104, no. C9, pp. 20713–20727, Sep. 1999.
- [23] V. U. Zavorotny and A. G. Voronovich, "Scattering of GPS signals from the ocean with wind remote sensing application," *IEEE Trans. Geosci. Remote Sens.*, vol. 38, no. 2, pp. 951–964, Mar. 2000.
- [24] T. Elfouhaily, D. R. Thomson, and L. Linstrom, "Delay-doppler analysis of bistatically reflected signals from the ocean surface: Theory and application," *IEEE Trans. Geosci. Remote Sens.*, vol. 40, no. 3, pp. 560–573, Mar. 2002.
- [25] C. Zuffada, A. Fung, J. Parker, M. Okolicanyi, and E. Huang, "Polarization properties of the GPS signal scattered off a wind-driven ocean," *IEEE Trans. Antennas Propag.*, vol. 52, no. 1, pp. 172–188, Jan. 2004.
- [26] D. Masters, V. U. Zavorotny, S. J. Katzberg, and W. Emery, "GPS signal scattering from land for moisture content determination," in *Proc. IEEE IGARSS*, Honolulu, HI, Jul. 24–28, 2000, pp. 3090–3092.
- [27] A. Komjathy, J. Maslanik, V. U. Zavorotny, P. Axelrad, and S. J. Katzberg, "Sea ice remote sensing using surface reflected GPS signals," in *Proc. IGARSS*, Honolulu, HI, Jul. 24–28, 2000, pp. 2855–2857.
- [28] S. T. Lowe, J. L. LaBrecque, C. Zuffada, L. J. Romans, L. E. Young, and G. A. Hajj, "First spaceborne observation of an Earth-reflected GPS signal," *Radio Sci.*, vol. 37, no. 1, pp. 7–17, Feb. 2002.
- [29] G. Beyerle and K. Hocke, "Observation and simulation of direct and reflected GPS signals in radio occultation experiments," *Geophys. Res. Lett.*, vol. 28, no. 9, pp. 1895–1898, 2001.
- [30] S. Gleason, S. Hodgart, Y. Sun, C. Gommenginger, S. Mackin, M. Adjrard, and M. Unwin, "Detection and processing of bistatically reflected GPS signals from low Earth orbit for the purpose of ocean remote sensing," *IEEE Trans. Geosci. Remote Sens.*, vol. 43, no. 6, pp. 1229–1241, Jun. 2005.
- [31] M. S. Braasch and A. J. Van Dierendonck, "GPS receiver architectures and measurements," *Proc. IEEE*, vol. 87, no. 1, pp. 48–64, Jan. 1999.
- [32] J. B. Tsui, *Fundamentals of Global Positioning System Receivers: A Software Approach*. Hoboken, NJ: Wiley, 1996.
- [33] ARINC. (2005, Dec.). "Navstar GPS Space Segment/Navigation User Interface," *GPS Joint Program Office*, Tech. Rep., drawing no: ICD-GPS-200, Revision D. [Online]. Available: <http://www.navcen.uscg.gov/gps/geninfo/IS-GPS-200D.pdf>
- [34] ——. (2005, Dec.). "Navstar GPS space segment/ user segment L5 interface," *GPS Joint Program Office*, Tech. Rep., drawing no: ICD-GPS-705. [Online]. Available: <http://www.navcen.uscg.gov/gps/modernization/Number.pdf>
- [35] *Global Positioning Products Handbook*, ZARLINK Semiconductors, Ottawa, ON, Canada, Aug. 1996.
- [36] *The TurboRogue Family of GPS Receivers User Manual. SNR-8000, SNR-8100, SNR-12, ICS-4000Z*, Allen Osborne Associates, Inc., Westlake Village, CA, Dec. 1995.
- [37] J. B. Thomas, *Signal-Processing Theory for the TurboRogue Receiver*. Pasadena, CA: JPL, 1995. Publ. 95-6.
- [38] *SONY High Speed Digital Data Recorder SIR-1000 Instruction Manual. SIR-1000i/SCX-32i 2-919-624-11 (2), Version 2003.8*, Sony Precision Technology, Inc, Canton, MI.
- [39] S. T. Lowe, P. Kroger, G. Franklin, J. L. LaBrecque, J. Lerma, M. Lough, M. R. Marcin, R. J. Muellerschoen, D. Spitzmesser, and L. E. Young, "A delay/doppler-mapping receiver system for GPS-reflection remote sensing," *IEEE Trans. Geosci. Remote Sens.*, vol. 40, no. 5, pp. 1150–1163, May 2002.
- [40] G. Heckler and J. L. Garrison, "Architecture of a reconfigurable software receiver," in *Proc. Inst. Navigation GNSS*, Long Beach, CA, Sep. 21–24, 2004, pp. 947–965.
- [41] H. You, J. L. Garrison, G. Heckler, and D. Smajlovic, "The autocorrelation of waveforms generated from ocean-scattered GPS signals," *IEEE Geosci. Remote Sens. Lett.*, vol. 3, no. 1, pp. 78–82, Jan. 2006.
- [42] O. Nogués-Correig, A. Sumpsi, A. Camps, and A. Rius, "A 3 GPS-channels doppler-delay receiver for remote sensing applications," in *Proc. IGARSS*, Toulouse, France, Jul. 21–25, 2003, pp. 4483–4485.
- [43] A. Sumpsi Colom, O. Nogués-Correig, and A. J. Camps Carmona, "Dispositivo de recepción DOPpler/DElay y almacenamiento de señales GPS," Spain Patent ES2 221 557A1, Dec. 16, 2004.
- [44] D. Akos, "Software radio architectures for GNSS," in *Proc. 2nd ESA Workshop Satellite Navigation User Equipment Technologies, (NAVITEC)*, Dec. 8–10, 2004.
- [45] S. Dunne and F. Soulat, "A GNSS-R coastal instrument to monitor tide and sea state," in *GNSS Reflection Workshop*. Guildford, U.K.: Surrey Univ., Jun. 9–10, 2005. [Online]. Available: <http://www.gnsr-05.com/presentations.html>
- [46] A. Brown and B. Mathews, "Remote sensing using bistatic GPS and a digital beam steering receiver," in *Proc. Inst. Navigation GNSS*, Long Beach, CA, Sep. 2005.
- [47] C. Kelley, J. Cheng, and J. Barnes, "Open source software for learning about GPS," in *ION GPS*, Portland, OR, Sep. 24–27, 2002. [Online]. Available: <http://home.earthlink.net/~cwkkelley/>
- [48] A. Helm, G. Beyerle, C. Reigber, and M. Rothacher, "The OpenGPS receiver: Remote monitoring of ocean heights by ground-based observations of reflected GPS signals," in *GNSS Reflection Workshop*. Guildford, U.K.: Surrey Univ., Jun. 9–10, 2005. [Online]. Available: <http://www.gnsr-05.com/presentations.html>
- [49] *OEM4 Family User Manual—Volume 1: Installation and Operation*, NovAtel Inc., Calgary, AB, Canada, Aug. 2004. OM-20000046 Rev 13. [Online]. Available: <http://www.novatel.com/Documents/Manuals/om-20000046.pdf>
- [50] *OEM4 Family. User Manual—Volume 2: Command and Log Reference*, NovAtel Inc., Calgary, AB, Canada, Aug. 2004. OM-20000047 Rev 13, this manual affects firmware version 2.200. [Online]. Available: <http://www.novatel.com/Documents/Manuals/om-20000047.pdf>
- [51] *Nios Development Board Reference Manual, Stratix Professional Edition*, Altera Corporation, San José, CA, Sep. 2004. [Online]. Available: http://www.altera.com/literature/manual/mnl_nios2_board_stratix_1s40.pdf
- [52] J. E. Volder, "The CORDIC trigonometric computing technique," *IEEE Trans. Electron. Comput.*, vol. EC-8, no. 3, pp. 330–334, Sep. 1959.
- [53] E. Cardellach, "Sea surface determination using GNSS reflected signals," Ph.D. dissertation, Univ. Politècnica de Catalunya (UPC)/Institut d'Estudis Espacials de Catalunya (IEEC), Barcelona, Spain, Mar. 2002.
- [54] *Global Positioning System: Theory and Applications*, J. J. Spilker, B. W. Parkinson, P. Axelrad, and P. Enge, Eds. Washington, DC: Amer. Inst. Aeronaut. Astronaut., 1996.



Oleguer Nogués-Correig received the M.Sc. degree in telecommunication engineering from the Polytechnic University of Catalonia (UPC), Catalonia, Spain, in 2002.

From July 2000 to March 2001, he worked as an Antenna Design Engineer for mobile applications with the Spanish firm FRACTUS S.A. From September 2001 to September 2002, he joined the Electromagnetics and Photonics Engineering Group at the Department of Signal Theory and Communications, UPC, designing and building the DO-DEREC

instrument, specially suited for the study of global navigation satellite system reflected signals (GNSS-R). Since December 2002, he has been a member of the Earth Observation Group at the Institut de Ciències de l'Espai, Institut d'Estudis Espacials de Catalunya (CSIC-IEEC). His current research interests include the design and development of new GNSS-R observation instruments, with applications in Earth science.



Estel Cardellach Galí received the B.S. degree in physics from The Autonomous University of Barcelona, Barcelona, Spain, in 1997 and the Ph.D. degree from the Polytechnic University of Catalonia, Catalonia, Spain, in 2002.

She has been working on scientific applications of GNSS for remote sensing of the Earth, mostly focused on assessing the geophysical information content of the GPS signals reflected off oceans. Besides scatterometric GPS applications, she developed an interferometric retrieval for polar ice altimetry

from atmospheric sounding data acquired during occulting GPS low Earth orbiters links, as a National Research Council Awardee for a postdoctoral position at NASA/Jet Propulsion Laboratory, Pasadena, CA (2002–2003). She has also been conducting studies on the geodetic uses of GNSS at the Harvard Smithsonian Center for Astrophysics, Cambridge, MA (2003–2005). She is currently a member of the research staff at the Institut de Ciències de l'Espai, Institut d'Estudis Espacials de Catalunya (CSIC-IEEC), Barcelona, Spain.



Josep Sanz Campderrós is currently working toward the B.S. degree in software engineering at the Polytechnic University of Catalonia, Catalonia, Spain.

From 2001 to 2005, he was a Software Developer with the Institut de Ciències de l'Espai, Institut d'Estudis Espacials de Catalunya (CSIC-IEEC). In 2005, he joined the Spanish firm IN2, where he worked as the Head of a software projects team. In January 2006, he started ENFASYSYSTEM S.L., Barcelona, Spain, which is a software development

company. He has been involved, freelance, in the development of many software projects, web applications, and Web sites for the Spanish industry and administration.



Antonio Rius received the Ph.D. degree in astrophysics from Barcelona University, Barcelona, Spain, in 1974.

From 1975 to 1985, he was a member of the technical staff at NASA's Deep Space Communications Complex, Madrid, Spain, where he was responsible for radio astronomical activities. Since 1986, he has been with the Spanish Consejo Superior de Investigaciones Científicas. He is currently responsible for the Earth Observation research group at the Institut de Ciències de l'Espai, Institut d'Estudis Espacials de Catalunya (CSIC-IEEC). His current research interests include applications to Earth science of GNSS.